

METAL ABUNDANCES OF KISS GALAXIES. IV. GALAXIAN LUMINOSITY-METALLICITY RELATIONS IN THE OPTICAL AND NEAR-IR

JOHN J. SALZER

Astronomy Department, Wesleyan University, Middletown, CT 06459; slaz@astro.wesleyan.edu

JANICE C. LEE

Steward Observatory, University of Arizona, 933 North Cherry Avenue, Tucson, AZ 85721; jlee@as.arizona.edu

JASON MELBOURNE

UCO/Lick Observatory, UC Santa Cruz, Santa Cruz, CA 95064; jmel@ucolick.org

JOANNAH L. HINZ AND ALMUDENA ALONSO-HERRERO¹

Steward Observatory, University of Arizona, 933 North Cherry Avenue, Tucson, AZ 85721; jhinz@as.arizona.edu; aalonso@as.arizona.edu

AND

ANNA JANGREN

Astronomy Department, Wesleyan University, Middletown, CT 06459; anna@astro.wesleyan.edu

Submitted 6 November 2004; Accepted 3 February 2005 – To appear in 20 May 2005 ApJ

ABSTRACT

We explore the galaxian luminosity-metallicity (L-Z) relationship in both the optical and the near-IR using a combination of optical photometric and spectroscopic observations from the KPNO International Spectroscopic Survey (KISS) and near-infrared photometry from the Two-micron All Sky Survey (2MASS). We supplement the 2MASS data with our own NIR photometry for a small number of lower-luminosity ELGs that are under-represented in the 2MASS database. Our B-band L-Z relationship includes 765 star-forming KISS galaxies with coarse abundance estimates from our follow-up spectra, while the correlation with KISS and 2MASS yields a total of 420 galaxies in our J-band L-Z relationship. We explore the effect that changing the correlation between the strong-line abundance diagnostic R_{23} and metallicity has on the derived L-Z relation. We find that the slope of the L-Z relationship decreases as the wavelength of the luminosity bandpass increases. We interpret this as being, at least in part, an effect of internal absorption in the host galaxy. Furthermore, the dispersion in the L-Z relation decreases for the NIR bands, suggesting that variations in internal absorption contribute significantly to the observed scatter. We propose that our NIR L-Z relations are more fundamental than the B-band relation, since they are largely free of absorption effects and the NIR luminosities are more directly related to the stellar mass of the galaxy than are the optical luminosities.

Subject headings: galaxies: abundances — galaxies: starburst

1. INTRODUCTION

Galaxies build up their content of heavy elements slowly over their lifetimes through well understood stellar-evolution processes. It has been known for at least twenty-five years that galaxies can exhibit different metallicity levels, with more massive galaxies having systematically higher abundances than dwarf galaxies (Lequeux *et al.* 1979). Understanding why these differences in metallicity exist is an important aspect of the study of galaxy evolution. The accurate assessment of the relationship between metallicity and mass provides an important constraint on the models of galaxy formation and evolution that attempt to account for the chemical evolution of the system (e.g., Prantzos & Boissier 2000; Boissier *et al.* 2003; Chiappini, Romano & Matteucci 2003; Riechick & Hensler 2003; Qian & Wasserburg 2004).

While it would be preferable to study the variation of metallicity with the mass of the galaxy, it is far more common for investigators to use luminosity as a surrogate for mass (e.g., Garnett & Shields 1987; Skillman, Kennicutt, & Hodge 1989; Zaritsky, Kennicutt, & Huchra 1994; Richer & McCall 1995; Garnett *et al.* 1997; Hidalgo-Gómez & Olofsson 1998; Kobulnicky & Zaritsky 1999; Pilyugin & Ferrini 2000; Melbourne & Salzer 2002; Lee *et al.* 2004; Lamareille *et al.* 2004). In nearly all of these previous studies, the authors find a strong correlation between luminosity and heavy element content. The latter is usually specified in terms of the relative abundance of oxygen to hydrogen for late-type and star-forming galaxies (where the metallicity is measured via nebular emission lines), and in terms of Fe/H for early-type galaxies (where the metallicity is assessed in terms of absorption-line indices). A few recent studies have considered the relationships between circular rotation speed and metallicity (Garnett 2002) and spectroscopic/photometric stellar mass estimates and metallicity (Tremonti *et al.* 2004, Pérez-González *et al.* 2003b), in order to try to tie the

¹ Present address: Departamento de Astrofísica Molecular e Infrarroja, IEM, Consejo Superior de Investigaciones Científicas, Serano 113b, 28006 Madrid, Spain.

observed variations in metal abundance to a more fundamental parameter (e.g., stellar or total mass).

There are a number of possible explanations for the observed variation of metal content with galaxian mass. For example, dwarf galaxies could, on average, be less efficient at converting their gas into stars, both now and in the past, and hence could simply have produced lower amounts of heavy elements in their lifetimes. Alternatively, it is possible that differences in the initial mass functions of galaxies as a function of either their metallicity or total mass could explain the observed trends. Both of these possibilities are brought into question by the observations of actively star-forming dwarf galaxies (a.k.a., blue compact dwarfs), that are seen to contain many high-mass stars capable of producing high levels of metal enrichment. For any reasonable assumed duty cycle of the star formation episodes in these galaxies, it would appear that they would readily produce enough heavy elements to give themselves relative abundances comparable to more massive galaxies. A key wild-card in the star-formation and metal enrichment in dwarfs is the observation that they have high gas-mass fractions relative to larger galaxies. Most of their “excess” gas lies at large radii, outside of the optical extent of the galaxy. If a mechanism existed to mix some of this gas into the central portion of the galaxy (e.g., tidal forces), it would serve to dilute the metallicity of the gas in the observable portion of the galaxy, and also to fuel further star formation.

A more likely explanation for the observed mass-metallicity and luminosity-metallicity (L-Z) relations is preferential loss of metal-enriched supernova ejecta. Low mass galaxies, with lower gravitational binding energies, are more apt to lose the metals produced in SNe explosions than are more massive galaxies. One can also explain the observed metallicity gradients in spiral disks via this mechanism. Simulations by Mac Low & Ferrara (1999) have shown that above some critical mass (roughly corresponding to a galaxy with $M_B = -12$), galaxies will lose a substantial amount of the metals they produce via a hot galaxian wind, while leaving most of the colder, ambient gas intact for the next generation of star formation. The extent of the metal loss via this supernova-driven wind varies with the mass of the galaxy, such that dwarfs lose much of their produced metals, while large spirals lose little if any. While the precise mechanism that causes the L-Z relation remains an open question, we will assume in the remainder of this paper, for the sake of discussion, that the hot galaxian wind model is the primary physical mechanism that produces the observed correlation between metallicity and luminosity/mass.

Recent work on the L-Z relation has begun to focus on trying to measure the change in the relation as a function of look-back time by studying galaxies at moderate redshifts (Kobulnicky & Zaritsky 1999; Contini *et al.* 2002; Kobulnicky *et al.* 2003; Lilly, Carollo & Stockton 2003; Maier, Meisenheimer & Hippelein 2004; Liang *et al.* 2004). Studying the evolution of the L-Z relation can be an alternate method for trying to quantify the evolution of the star-formation rate density. Since the evolution of metal abundance, particularly in high-mass galaxies where the effect of galaxian winds is less important, must correlate with the star-formation history of massive stars,

the evaluation of the change in the L-Z relation with look-back time provides a powerful tool for measuring the star-formation history of the universe back to $z = 1$ (and possibly further).

Melbourne & Salzer (2002; Paper I) have previously used the star-forming galaxies discovered in the KPNO International Spectroscopic Survey (KISS; Salzer *et al.* 2000) to explore the nature of the L-Z relation for a large ($N = 519$) sample of emission-line galaxies (ELGs). In the current paper, we extend that study by including a larger sample of galaxies for which coarse abundance estimates are available, and by investigating the L-Z relation in a range of bandpasses from B to K. By considering the L-Z relation in the near-IR, we are able to substantially reduce (eliminate?) the effects of internal absorption on the derived result. In addition, we have revised our coarse abundance calibration, taking into account recently obtained spectral data. An added advantage of the current study is that we use a large sample of galaxies with *homogeneous* data (both spectroscopic and photometric). Some previous studies have suffered from using data taken from multiple sources, where the abundances were not always derived in a consistent fashion.

The paper is laid out as follows. Section 2 describes the various optical and NIR datasets used for this study, including the presentation of new H and K band imaging photometry obtained for this project. Section 3 details our method of deriving coarse metallicity estimates for the KISS ELGs, and includes a redetermination of the metallicity - line ratio relations first presented in Paper I. In Section 4 we present our new L-Z relations for five photometric bands (BVJHK), while §5 presents a discussion of our findings. These include a comparison with previous work, including recent determinations of the L-Z relation at higher redshifts, as well as a discussion of the scatter in our relation. The results of this paper are summarized in §6. Throughout this paper, a value for the Hubble constant of $75 \text{ km s}^{-1} \text{ Mpc}^{-1}$ is assumed.

2. OBSERVATIONAL DATA

To explore the questions raised above, we utilize the large sample of star-forming galaxies cataloged by the KPNO International Spectroscopic Survey (KISS; Salzer *et al.* 2000). To date, KISS has generated three lists of emission-line selected galaxies. The larger portion of the survey is made up of galaxies selected via the presence of the $H\alpha$ line in their objective-prism spectra. These are cataloged in Salzer *et al.* (2001; hereafter KR1) and Gronwall *et al.* (2004a; hereafter KR2), and include 2158 emission-line galaxy (ELG) candidates. The third list is made up of objects selected due to the presence of $[O \text{ III}]\lambda 5007$ (Salzer *et al.* 2002; hereafter KB1), and has a total of 223 objects cataloged. The $[O \text{ III}]$ -selected ELGs in KB1 tend to be lower in luminosity, on average, than the $H\alpha$ -selected galaxies in KR1 and KR2. However, there is substantial overlap in the sky coverage of the KR1 and KB1 surveys, and essentially all of the KB1 objects in the overlap regions are also detected in KR1. This suggests that there is no significant bias introduced by combining the $H\alpha$ -selected and $[O \text{ III}]$ -selected ELGs. The total number of unique ELGs tabulated in the three lists is 2266.

The current study makes use of a large amount of observational data, obtained from a number of different

sources. We describe below the make-up of our dataset.

2.1. KISS Optical Photometry and Spectroscopy

The basic data in the KISS catalogs include accurate astrometry (typical uncertainties of 0.25 - 0.30 arcsec in RA and Dec) and calibrated B & V photometry for each object in the catalog. The latter have typical uncertainties of 0.06 mag for B = 16 galaxies, increasing to 0.09 mag at B = 19 (Salzer *et al.* 2000). In addition, the objective-prism data provide estimates of the redshift of each ELG, plus a measurement of its line flux and equivalent width. These spectral data are too coarse to allow for the determination of activity types (e.g., star-forming vs. AGN), so follow-up spectra are needed to maximize the scientific usefulness of the survey. Members of the KISS group have been engaged in a campaign of “quick-look” spectroscopy of the ELG candidates for the past several years. To date, observations have been obtained for 1351 KISS ELGs, including all 223 of the [O III]-selected KB1 list, 935 of 1128 (83%) ELGs from the H α -selected KR1 catalog, and 307 of 1029 (30%) of the candidates from KR2. For the analysis carried out in this paper, we use only spectra from star-forming galaxies that have spectral data of high enough quality to insure accurate emission-line ratios (i.e., galaxies with spectral quality codes of 1 or 2 as tabulated in the spectral data papers listed below). After removing all of the AGNs (Seyfert 1s and 2s, LINERs, and QSOs), those objects with lower spectral quality, and the roughly 9% of KISS candidates that turn out to not be actual ELGs, we are left with a final sample for the current paper of 766 star-forming ELGs.

The follow-up spectra have been obtained with a variety of telescopes and spectrographs. The details of the observational set-ups and measured spectral parameters are given in a series of existing or planned future papers, each of which presents data from a specific telescope. These include the Hobby-Eberly 9.2-m telescope (Gronwall *et al.* 2004b), the Lick 3.0-m (Melbourne *et al.* 2004; Paper II), the MDM 2.4-m (Wegner *et al.* 2003), the WIYN 3.5-m with the Hydra multi-fiber positioner, the ARC 3.5-m, and the KPNO 2.1-m telescope. With the exception of the WIYN 3.5-m spectra, all data were obtained using long slits with widths of 1.5 - 2.0 arcsecs. The WIYN spectra were taken through 2 arcsec diameter fibers. The quick-look spectra exhibit a range of S/N ratios. Some spectra cover the full optical spectral range (from below [O II] $\lambda\lambda$ 3726,3729 to above [S II] $\lambda\lambda$ 6717,6731), although the majority of our data do not go below 4000 Å, usually due to limitations of the spectrographs that were available. At a minimum, all of our spectra include the H β , H α , [O III] $\lambda\lambda$ 4959,5007, and [N II] $\lambda\lambda$ 6548,6583 lines. In addition, the follow-up spectra provide us with an estimate of the Balmer decrement reddening parameter $c_{H\beta}$, plus an accurate redshift. The latter, along with our broad-band photometry from the original survey data, allow us to compute absolute magnitudes for each ELG. The emission-line fluxes are used to estimate the oxygen abundance, using the method described in §3.

2.2. 2MASS NIR Photometry

In order to explore the near-IR L-Z relationship, we take advantage of the Two-micron All-Sky Survey² (2MASS). We have correlated the positions of all 2266 KISS ELGs in the first three survey lists (KR1, KR2, KB1) with both the 2MASS point-source and extended-source catalogs. We have found 2MASS detections for 1479 of the KISS ELGs (65.3%). In most cases, the KISS galaxies were detected in all three 2MASS bands (J, H, and K), although for some sources near the 2MASS flux limit the KISS ELGs were detected in only one (usually J) or two (usually J & H) filters. The median formal magnitude uncertainties for the 2MASS-detected KISS galaxies are 0.10 mag for J, 0.13 mag for H, and 0.15 mag for K. The full details of our correlation procedure, as well as a description of the NIR properties of the KISS ELGs is given in A. Jangren *et al.* (2005b, in preparation). In the current paper we simply utilize the cataloged 2MASS JHK photometry to compute NIR absolute magnitudes for all of the detected ELGs.

2.3. Steward NIR Observations

As discussed in A. Jangren *et al.* (2005b, in preparation), the 2MASS survey was quite efficient at detecting the more luminous star-forming galaxies and AGNs in the KISS catalogs. However, the lower luminosity ELGs are systematically under-represented in 2MASS. This comes about for two reasons. First, since the detection limit of the 2MASS project is not as deep as that for KISS, a substantial portion of the KISS dwarf population is not within the sensitivity limits of 2MASS. Second, the colors of the low-luminosity star-forming ELGs are much bluer than are the more luminous KISS galaxies. Hence, at a given optical magnitude, the more luminous (redder) ELGs are more likely to be detected in the NIR than the bluer dwarf galaxies. The net effect is that the majority of the lower luminosity KISS ELGs ($M_B > -18.0$) are not detected by 2MASS.

To supplement the sparse 2MASS photometry available for the low-luminosity galaxies of the KISS sample, we have carried out near-IR observations for some of our lowest luminosity galaxies. Our original intent was to obtain both K_s and H band imaging for all 52 galaxies with $M_B > -17.0$ in the KR1 catalog. Due to unusual difficulties with weather, however, only a fraction of this sample was observed. For the purposes of constructing the luminosity-metallicity relationship using coarse abundances, the inclusion of this limited set of near-IR photometry is still sufficient to improve our statistics in the low-luminosity portion of the distribution. Thus, we have simply abridged the original project and present the available data here.

H-band images were obtained with a NICMOS3 256 × 256 camera at the Steward Observatory 2.3m Bok Telescope on Kitt Peak in June 2002. This MOSFET array has a pixel scale of 0".60 pixel⁻¹ and a 2'.56 square field of view when used at the f/45 focus.

K_s images were obtained with the PISCES camera

² This publication makes use of data products from the Two-micron All-Sky Survey, which is a joint project of the University of Massachusetts and the Infrared Processing and Analysis Center/California Institute of Technology, funded by the National Aeronautics and Space Administration and the National Science Foundation.

(McCarthy et al. 2001) at the 6.5m MMT³ on Mount Hopkins in April 2003. PISCES uses a 1024×1024 pixel HAWAII (HgCdTe) detector (Kozlowski et al. 1994; Hodapp et al. 1996) and operates at the f/9 focus at the MMT, with a resultant pixel scale of $0''.185 \text{ pixel}^{-1}$ and circular field of view with a $3'/16$ diameter.

At both observatories we followed the same standard near-IR observing sequence. A series of on-source short exposures were taken for each target, with dithering offsets applied after every frame and the integration time (~ 30 s) of each frame determined by the level of the sky background count rate. Since the targets had diameters on the order of $10''$ or smaller and the surrounding fields were relatively sparse, it was not necessary to move the target completely off the detector to obtain separate blank sky images for flat-fielding and sky-subtraction purposes. Total integration times varied between 10 and 20 minutes for each target.

Standard near-IR reductions were performed using the Image Reduction and Analysis Facility⁴ (IRAF). Average dark frames were subtracted, bad pixel masks were applied, and the images were flat-fielded using a normalized median combination of the 5 to 10 temporally closest frames. For the PISCES data, corrections for cross-talk between quadrants and geometric distortion were also applied. Finally, the individual short exposure frames for each target were aligned and combined. Flux calibration was performed using standard stars from the UKIRT list for data from the Bok Telescope and from the Persson et al. (1998) list for data from the MMT, and the canonical atmospheric extinction coefficients of 0.04 mag airmass⁻¹ at H and 0.08 mag airmass⁻¹ at K_s were used to calculate zero-points for each night. The uncertainty in the airmass correction was minimized by ensuring that all standard and galaxy observations were made at low airmass (1.2 airmasses on average) and over the narrowest range of airmass that was practical (~ 0.25).

Photometry was performed using the IRAF APPHOT routine and total magnitudes were measured by using circular apertures large enough to encompass all the light from the target. Our results are listed in Table 1. The quoted errors were computed following Pérez-González et al. (2003a). Average total errors are 0.07 mag for the MMT K_s photometry and 0.3 mag for the Bok H-band photometry. The larger errors in the Bok data are primarily due to a greater uncertainty in the sky determination due to the high and rapidly fluctuating background count rate at the time of the observations. For the MMT PISCES data, we have also measured field stars in our science images for which reliable photometry is also available from the 2MASS PCS. There were typically one to two stars per field that could be used for this type of comparison. The differences between our measured values and those from 2MASS were consistently within 1.5σ of the quoted 2MASS errors, validating the photometric calibrations that were applied.

3. METALLICITIES OF THE KISS GALAXIES

³ The MMT Observatory is a joint facility of the University of Arizona and the Smithsonian Institution.

⁴ IRAF is distributed by the National Optical Astronomy Observatories, which are operated by AURA, Inc. under cooperative agreement with the National Science Foundation.

The metallicity (defined here as $12 + \log(\text{O}/\text{H})$) of nebular star-forming regions can be calculated from ratios of the [O III] and [O II] spectral lines relative to a Balmer line of hydrogen (Osterbrock 1989; de Robertis 1987). This requires high signal-to-noise ratio spectra and the detection of the oxygen auroral line [O III] $\lambda 4363$ to estimate electron temperature in the nebula. We term this abundance measurement method the T_e method. The strength of the auroral line is usually 50-200 times weaker than [O III] $\lambda 5007$, making it difficult to observe. To make matters worse, if the metallicity of the star-forming region is larger than $12 + \log(\text{O}/\text{H}) \sim 8$, the [O III] line strengths and the [O III] $\lambda 4363$ /[O III] $\lambda 5007$ ratio decline with increasing oxygen abundance, making the detection of the auroral line impossible for high metallicity targets at modest redshifts. In order to estimate the metallicity for cases where [O III] $\lambda 4363$ is not observed, empirical relations between ratios of the strong oxygen lines ([O III] $\lambda \lambda 5007, 4959$ and [O II] $\lambda \lambda 3726, 3729$) and metallicity are calibrated using HII regions in the Milky Way and local galaxies. These so-called R_{23} methods (Edmunds and Pagel 1984; Zaritsky et al. 1994; Kobulnicky et al. 1999; Pilyugin 2000, 2001) have typical metallicity uncertainties of ~ 0.1 – 0.2 dex, as compared to uncertainties of ~ 0.01 – 0.04 dex that are typically obtained via the T_e method. The recent study by Kewley & Dopita (2002) has refined the strategies for deriving metal abundances making use of the strongest nebular lines present in the spectrum of star-forming galaxies.

The follow-up spectra of a typical KISS emission-line galaxy generally contain detections of the $H\alpha$, $H\beta$, [O III] $\lambda 5007$, and [N II] $\lambda 6583$ lines. However, due to limited spectral coverage and to the sometimes low signal-to-noise ratio (S/N) of the quick-look spectra, they often do not contain the additional lines necessary for accurate metal abundances, such as [O III] $\lambda 4363$ (T_e abundances) or [O II] $\lambda \lambda 3726, 3729$ (T_e and R_{23} abundances). In particular, the absence of the [O II] doublet precludes our using any of the strong-line ratios proposed by Kewley & Dopita (2002). Rather than abandon these objects, we define an empirical calibration between metallicity and the strong lines available in the bulk of our spectra. These calibrations result from metallicity measurements of a subset of the KISS galaxies for which we can either calculate a T_e abundance or an R_{23} abundance. The process was first carried out in Paper I. In the current paper we update the calibrations with additional T_e and R_{23} abundance measurements, and we apply the calibrations to a larger set of follow-up spectra in order to determine global luminosity-metallicity relations for KISS galaxies. A brief description of the data sets used and their application to the strong-line metallicity calibration is given below. For a more detailed discussion of the process please refer to Paper I.

3.1. T_e Metal Abundances

The KISS team has obtained high S/N spectra of 25 low metal abundance galaxies using the Lick 3.0-m telescope and the 6.5-m MMT. Each spectrum includes a detection of [O III] $\lambda 4363$, which we use to measure the electron temperature of the nebula. An estimate of the electron density comes from the [SII] line ratio. Metal abundances are calculated using the IRAF NEBULAR package (de Robertis et al. 1997; Shaw & Du-

four 1995). The abundance results are presented in a series of papers (Melbourne *et al.* 2004 (Paper II); Lee *et al.* 2004 (Paper III)), and are summarized in Table 2. Columns 1 and 2 give the KISSR and/or KISSB numbers of the galaxies. Column 3 shows the logarithm of the $([\text{N II}]\lambda 6583/\text{H}\alpha)$ line ratios, while columns 4 and 5 are $\log([\text{O II}]\lambda\lambda 3726, 3729/\text{H}\beta)$ and $\log([\text{O III}]\lambda 5007/\text{H}\beta)$ respectively. Column 6 gives the resulting T_e metallicity. Please refer to Papers II and III for full details.

3.2. R_{23} Metal Abundances

In addition to the high signal-to-noise ratio spectra discussed above, the KISS team has gathered spectra of 185 galaxies that contain both the strong $[\text{O III}]\lambda 5007$ and $[\text{O II}]\lambda\lambda 3726, 3729$ lines allowing an R_{23} -style metallicity measurement for each. The relation between $R_{23} = \frac{f([\text{O III}]\lambda\lambda 4959, 5007) + f([\text{O II}]\lambda\lambda 3727, 29)}{f(\text{H}\beta)}$ and metallicity has been calibrated with a combination of T_e observations of starburst galaxies and star-forming regions in nearby galaxies for the lower abundances, and photoionization models for the higher metallicities (e.g., Stasinska 1990; McGaugh 1991; Oey & Kennicutt 1993; Kewley & Dopita 2002). The relationship is double valued. On the lower-metallicity branch ($12 + \log(\text{O}/\text{H}) < 7.9$), metallicity increases as R_{23} increases. R_{23} decreases with increasing metallicity for metal abundances greater than ~ 8.1 , the upper-metallicity branch. Objects in between are called turn-around region galaxies.

After calculating R_{23} for each object in our sample we identify which branch of the metallicity relation the galaxy lies on. As outlined in Paper I, objects with $\log([\text{N II}]\lambda 6583/\text{H}\alpha) < -1.3$ are assigned to the low-metallicity branch, while objects with $\log([\text{N II}]\lambda 6583/\text{H}\alpha) > -1.0$ are assigned to the high metallicity branch. Those objects with nitrogen line ratios between these constraints are assigned to the turn-around region of the R_{23} relation and no metallicity is calculated. As an additional constraint, we find that objects with low signal-to-noise ratio in the $\text{H}\beta$ line do not produce reliable metal abundances from R_{23} methods. The uncertainty in $\text{H}\beta$ propagates through the metallicity determination by means of the reddening coefficient $c_{\text{H}\beta}$. We limit our metallicity calculations to those objects with equivalent width of $\text{H}\beta > 8 \text{ \AA}$. Objects below this cutoff tend to have unphysical $[\text{O III}]/[\text{O II}]$ line ratios (Paper I).

3.2.1. Lower-Metallicity Branch Calibration

For objects on the lower-metallicity branch, we adopt the Pilyugin (2000) calibration of R_{23} called the $p3$ method:

$$12 + \log(\text{O}/\text{H}) = 6.35 + 1.45X_3^*, \quad (1)$$

where $X_3^* = -1.20\log(f([\text{O III}]\lambda\lambda 4959, 5007)/f(\text{H}\beta)) + 2.20\log(R_{23})$. This equation reproduces T_e abundance results to within 0.1 dex. We calculate $p3$ metallicities for 17 galaxies with metal abundances that range from 7.6 to 8.2. The abundance results are given in Table 3. Columns 1 and 2 give the KISSR and KISSB numbers of the galaxies. Column 3 is $\log([\text{N II}]\lambda 6583/\text{H}\alpha)$, while columns 4 and 5 are $\log([\text{O II}]\lambda\lambda 3726, 3729/\text{H}\beta)$ and $\log([\text{O III}]\lambda 5007/\text{H}\beta)$ respectively. Column 6 gives

the resulting $p3$ metallicity. We assign a standard uncertainty to the metallicity measurements of 0.1 dex (Paper I).

3.2.2. Upper-Metallicity Branch Calibrations

For objects on the upper-metallicity branch, we originally adopted the Edmunds & Pagel (1984; hereafter EP) fit, as quoted in Pilyugin (2000):

$$12 + \log(\text{O}/\text{H}) = 9.57 - 1.38\log(R_{23}). \quad (2)$$

This fit differs only marginally from the one presented by Pilyugin (being ~ 0.08 dex higher). Table 4 reports the metallicity results for the R_{23} method. 47 galaxies are measured with metal abundances ranging from 8.2 to 9.5. The first six columns are the same as in Table 3, except that the last column reports the metal abundances derived from the R_{23} equation above. The R_{23} calibration has a larger inherent scatter with metallicity than does the $p3$ calibration; we estimate an uncertainty of 0.15 dex for these measurements (Paper I).

Our adopted upper-branch R_{23} relationship defines the abundance scale for the luminous galaxies used in the analysis presented in this paper. The use of a different R_{23} relationship could potentially have a dramatic impact on the slope of the derived L-Z relation. It should be stressed that there are a number of different calibrations of the R_{23} relation in the literature (e.g., EP; McCall, Rybski & Shields 1985; McGaugh 1991; Zaritsky *et al.* 1994; Kobulnicky *et al.* 1999; Pilyugin 2000, 2001), some of which differ significantly from each other. We have adopted the EP version, which falls roughly mid-range of the other versions of the relation. Paper I considered the effect that using a different R_{23} relation would have on the slope of the L-Z relation, and concluded that it could have only a modest effect (probably in the range of 5-10%). However, we felt that it was important to revisit this question in somewhat more detail by considering a few additional R_{23} relations.

Recent measurements of T_e abundances for objects on the upper branch of the R_{23} relationship by Kennicutt, Bresolin & Garnett (2003; hereafter KBG) lie well below the R_{23} calibrations suggested in previous studies, including the one by EP adopted above (see Figure 12 of KBG). The implication of this result is that abundances derived using one of these older R_{23} relationships could be substantially higher than their actual values. We used the data presented in KBG to derive an alternate fit for the upper branch of the R_{23} relationship:

$$12 + \log(\text{O}/\text{H}) = 9.31 - 1.38\log(R_{23}). \quad (3)$$

Note that the slope is identical to the Edmunds & Pagel value, but the intercept is 0.26 dex lower. Since a lower abundance calibration for the R_{23} relationship could potentially lead to a substantially shallower L-Z slope, we decided to recompute our coarse abundance calibration using this new relation. The R_{23} abundances derived for our sample using the KBG relation are given in column 7 of Table 4.

Finally, we have used the analytical fit to the R_{23} – metallicity relation obtained by Tremonti *et al.* (2004) for SDSS data (their Equation 1) as a third independent calibration of the method. Column 8 of Table 4 presents values for the R_{23} abundances computed using the Tremonti *et al.* relation (hereafter referred to as the

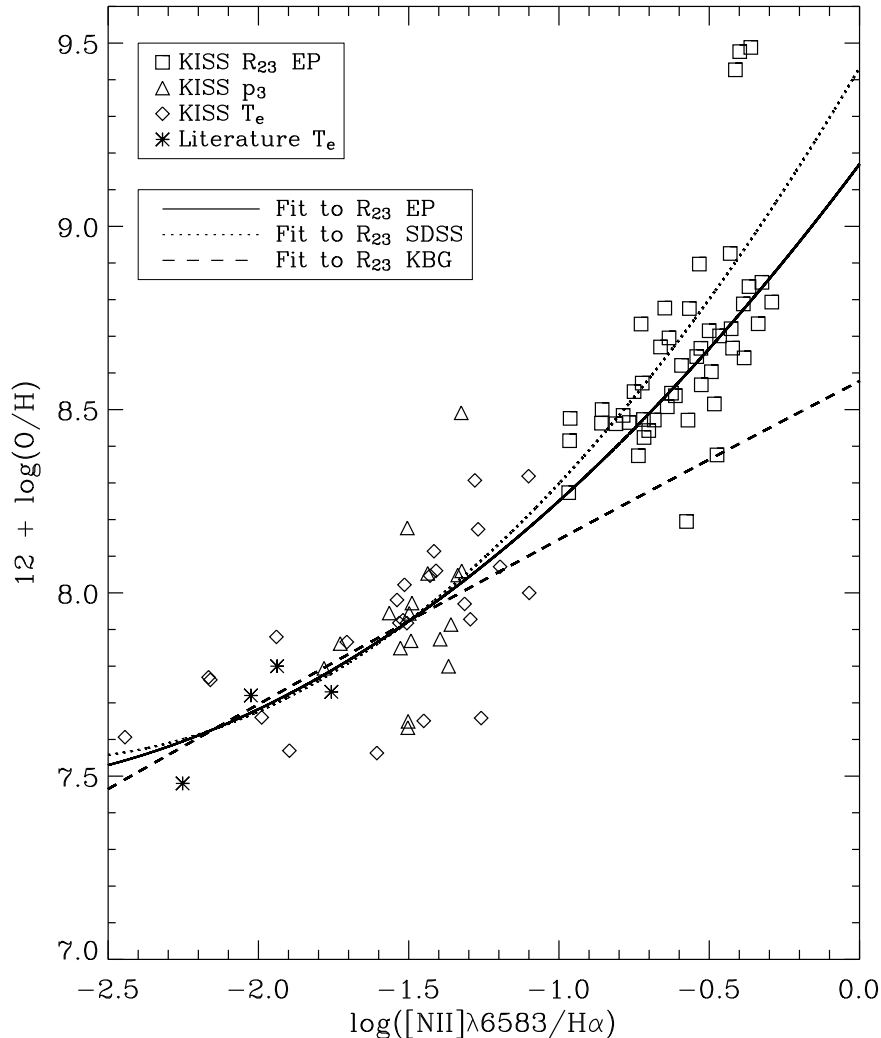


FIG. 1.— This figure relates the $[\text{N II}]\lambda 6583/\text{H}\alpha$ line ratio to metallicity. Abundances calculated using the EP R_{23} fit are shown as squares, while p_3 abundances are shown as triangles. Abundances calculated with the T_3 method are shown as diamonds. T_e abundance data taken from Izotov *et al.* (1997) are shown as asterisks. We fit a quadratic function to the data (solid line). In addition, we plot the quadratic fits to the abundance data computed using the SDSS and KBG R_{23} calibrations (dotted line and dashed line, respectively). See text for details.

SDSS relation). In the following sections, we utilize all three of these R_{23} relations to calibrate our coarse abundance method and further explore the impact of different R_{23} calibrations on the derived L-Z relation.

3.3. Coarse Metal Abundance Estimates

Using the T_e , p_3 and R_{23} metal abundance estimates described above, we calibrate empirical relations between two sets of strong emission-line ratios ($[\text{N II}]\lambda 6583/\text{H}\alpha$, $[\text{O III}]\lambda 5007/\text{H}\beta$) and metallicity. We then estimate metal abundances for the large sample of KISS galaxies that have high quality follow-up spectra. Figure 1 shows how the $[\text{N II}]\lambda 6583/\text{H}\alpha$ line ratio varies with metallicity, while Figure 2 shows the same for the $[\text{O III}]\lambda 5007/\text{H}\beta$ line ratio. For each plot, the diamonds are T_e abundance measurements, triangles are p_3 abundances, and squares are R_{23} measurements. For the latter we use the abundances computed using the EP R_{23} calibration for the purpose of illustration. Asterisks represent objects taken

from Izotov *et al.* (1997). These objects are included to increase the number of low-metallicity galaxies available, in order to better constrain the resulting fit (as in Paper I).

Our coarse abundance relations are determined by fitting low-order polynomials to the data shown in Figures 1 and 2. We carry out the fitting process separately for the three choices of the R_{23} relation described above. For the $[\text{N II}]/\text{H}\alpha$ – metallicity data we fit a second order polynomial to those objects with $\log([\text{N II}]\lambda 6583/\text{H}\alpha) < -0.45$, where the line ratio is well behaved with respect to metallicity. The fit is of the form

$$12 + \log(O/H) = A + B \cdot N + C \cdot N^2, \quad (4)$$

$$N = \log([\text{N II}]\lambda 6583/\text{H}\alpha).$$

The polynomial coefficients and their formal uncertainties are given in Table 5. Also listed in the table are the RMS scatters about the fits. The latter lie in the range 0.13 to 0.16 dex, and are adopted as the formal uncertainties in the abundance estimates obtained from this

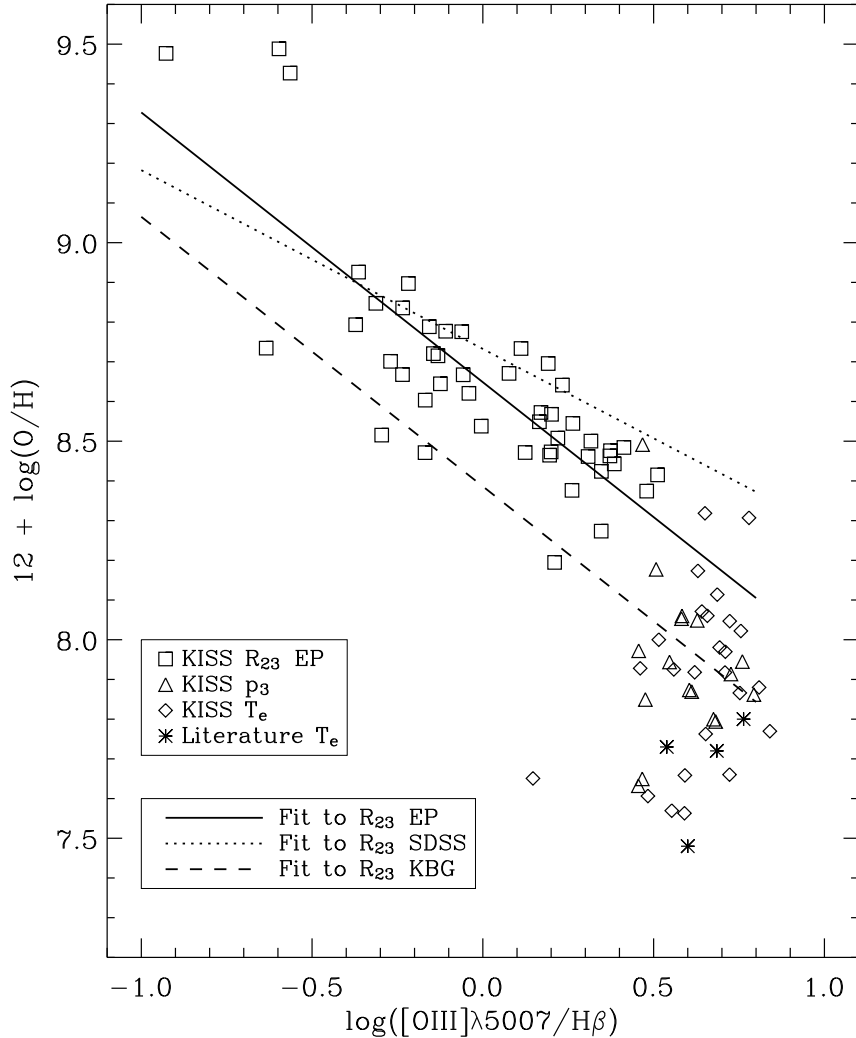


FIG. 2.— This figure relates the $[\text{O III}]\lambda 5007/\text{H}\beta$ line ratio to metallicity. Abundances calculated using the EP R_{23} fit are shown as squares, while p_3 abundances are shown as triangles. Abundances calculated with the T_3 method are shown as diamonds. T_e abundance data taken from Izotov *et al.* (1997) are shown as asterisks. We fit a line to the high metallicity branch (solid line). In addition, we plot the linear fits to the abundance data computed using the SDSS and KBG R_{23} calibrations (dotted line and dashed line, respectively). See text for details.

equation. Note that the objects with high abundances ($12 + \log(\text{O}/\text{H}) > 9.0$) are excluded from the fit. These are objects found in the lower right portion of the diagnostic diagram shown in Figure 3, where the $[\text{N II}]/\text{H}\alpha$ ratio is no longer sensitive to changes in metallicity.

We plot the three fits in Figure 1. The solid line is the fit to the abundances derived with the EP R_{23} relation (corresponding to the data plotted in the figure), while the dashed and dotted lines show the fits to the KBG and SDSS relations (data points not plotted). All three fits agree well with each other on the left side of the diagram, where the $[\text{N II}]/\text{H}\alpha$ ratio is most sensitive to metal abundance (see below), but diverge on the right side due to the different R_{23} abundance determinations. The KBG R_{23} abundances are systematically lower than the EP ones by 0.26 dex, leading to the flatter $[\text{N II}]/\text{H}\alpha$ – metallicity relation seen in the figure. On the other hand, the SDSS fit agrees more closely with the EP relation, being only slightly steeper at the high-abundance

end.

For the $[\text{O III}]/\text{H}\beta$ – metallicity data we fit a linear relation to the objects located on the upper-metallicity branch of the R_{23} relation ($\log([\text{N II}]\lambda 6583/\text{H}\alpha) > -1.2$). The fit is of the form

$$12 + \log(\text{O}/\text{H}) = A + B \cdot O, \quad (5)$$

$$O = \log([\text{O III}]\lambda 5007/\text{H}\beta).$$

The three different data sets are fitted separately, and the resulting polynomial coefficients are given in Table 5. In this case the scatter about the fits ranges between 0.11 and 0.14, comparable to the values found for the $[\text{N II}]/\text{H}\alpha$ relation. Figure 2 plots the three fits, using the same conventions employed in Figure 1. Since the fits are only to the upper branch objects, they more directly reflect the differences in the input R_{23} relations. The KBG fit is parallel to, but offset from, the EP fit, while the SDSS fit predicts lower abundances than EP for the most metal-rich galaxies (left side of diagram)

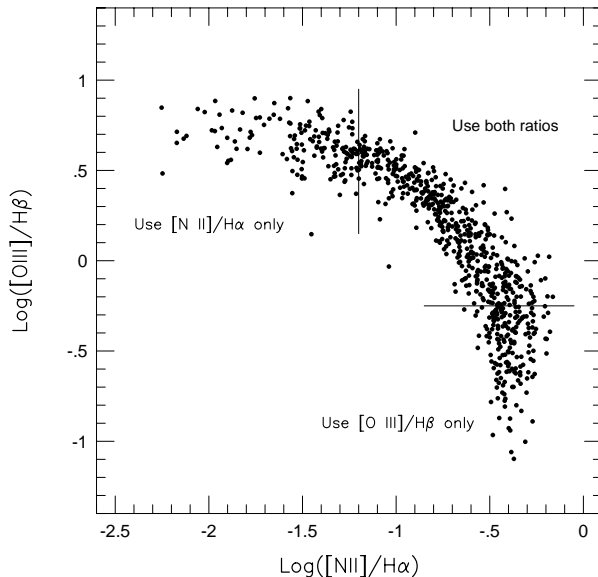


FIG. 3.— A traditional emission-line diagnostic diagram plotting $[\text{O III}]/\text{H}\beta$ vs. $[\text{N II}]/\text{H}\alpha$. Only KISS star-forming galaxies for which a coarse abundance estimate has been derived are included. The three regimes described in the text for specifying how the coarse abundances are computed are indicated.

and higher abundances than EP for galaxies with intermediate abundances.

Armed with these relations, we calculate metal abundances for the large sample of KISS galaxies with high-quality follow-up spectra in the following way. For galaxies with $\log([\text{N II}]\lambda 6583/\text{H}\alpha) < -1.2$ we calculate the metallicity using only the nitrogen line ratio and Equation 4. For galaxies with $\log([\text{N II}]\lambda 6583/\text{H}\alpha) > -1.2$ and $\log([\text{O III}]\lambda 5007/\text{H}\beta) > -0.25$ we calculate metallicities using both the nitrogen and oxygen line ratios and equations 4 and 5. We take the average of the two results to produce a final abundance estimate. For objects with $\log([\text{O III}]\lambda 5007/\text{H}\beta) < -0.25$, we use only the oxygen line ratio and Equation 5 to calculate metallicity. In Figure 3 we plot a standard emission-line diagnostic diagram of $[\text{O III}]/\text{H}\beta$ vs. $[\text{N II}]/\text{H}\alpha$, and indicate the three regions specified above. In this diagram, the metallicity of the galaxies increases smoothly from the upper left to the lower right. It should be clear from the diagram that the $[\text{O III}]/\text{H}\beta$ becomes insensitive to changes in metallicity at small values of $[\text{N II}]/\text{H}\alpha$, while the $[\text{N II}]/\text{H}\alpha$ ratio is not a good abundance indicator at small values of $[\text{O III}]/\text{H}\beta$.

The above relations update and replace the corresponding versions from Paper I. The fit to the EP oxygen-metallicity plot is very similar to that from our previous paper, while the EP nitrogen-metallicity relation has changed slightly at the low abundance end. For objects with $\log([\text{N II}]/\text{H}\alpha) = -2.0$, our new relation leads to abundances that are 0.07 dex higher, while at $\log([\text{N II}]/\text{H}\alpha) = -1.2$, the revised relation predicts metallicities that are 0.03 dex higher than the old relation. Pettini & Pagel (2004) carry out an analysis very similar to ours for the $[\text{N II}]/\text{H}\alpha$ ratio, and arrive at a relation reminiscent of our equation 4. Their relation pre-

dicts oxygen abundances that are roughly 0.1 dex higher than those provided by our equation 4 (for all three R_{23} calibrations) for $\log([\text{N II}]/\text{H}\alpha)$ less than -1.0 , and comparable to our EP values for higher $[\text{N II}]/\text{H}\alpha$ ratios.

4. OPTICAL AND NIR METALLICITY-LUMINOSITY RELATIONS

4.1. Presentation of new L-Z relations

Following the procedures described in the previous section, we are able to compute coarse oxygen abundances for 766 KISS star-forming galaxies. This represents a roughly 50% increase over the number of KISS ELGs with coarse abundances available for the study carried out in Paper I. Only galaxies whose follow-up spectra provide high-quality measurements for the $[\text{O III}]/\text{H}\beta$ and $[\text{N II}]/\text{H}\alpha$ line ratios are used. This entire dataset also possesses B and V photometry, and more than half were detected by 2MASS and have NIR magnitudes. In this section we present luminosity-metallicity relations for the KISS ELGs in five different photometric bands.

In order to better illustrate the nature of our large sample of star-forming ELGs, we display in Figure 4 plots of a number of measured physical parameters. The four panels plot the following parameters against B-band absolute magnitude: (a) B–V color, (b) the Balmer decrement reddening parameter $c_{H\beta}$, (c) the logarithm of the $\text{H}\alpha$ equivalent width (in \AA , measured from our follow-up spectra), and (d) the logarithm of the $\text{H}\alpha$ line luminosity (in ergs/s). In all panels, filled symbols reflect objects detected by 2MASS in the J band, while open symbols indicate those that are not detected in the NIR. One sees expected/familiar trends in all plots: the galaxies tend toward bluer colors, lower amounts of absorption, higher equivalent width emission, and lower line luminosities in progressing from higher to lower luminosities.

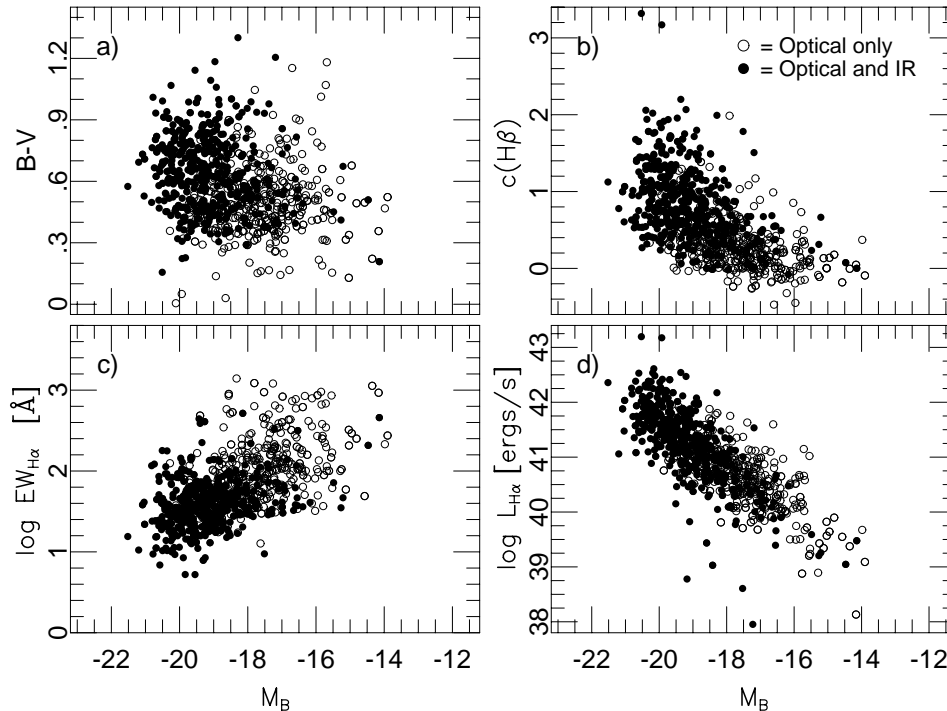


FIG. 4.— Measured physical parameters for the KISS star-forming ELGs used in this paper to construct our L-Z relations, plotted as a function of B-band absolute magnitude: (a) B–V color; (b) the Balmer decrement reddening parameter $c_{H\beta}$; (c) the logarithm of the H α equivalent width (in \AA , measured from our follow-up spectra); and (d) the logarithm of the H α line luminosity (in ergs/s). In all panels, filled symbols reflect objects detected by 2MASS in the J band, while open symbols indicate those that are not detected in the NIR. Note the tendency for the lower luminosity galaxies to not be detected in the NIR.

A key thing to note is the tendency for the lower luminosity galaxies to not be detected in the NIR: at luminosities above $M_B = -20.0$, 96.8% of the KISS ELGs are 2MASS detected, while for $M_B > -18.0$, only 20.4% have measurable 2MASS fluxes. A more complete description of the properties of the KISS ELGs can be found in L. Chomiuk *et al.* (2005, in preparation) and A. Jangren *et al.* (2005a, in preparation).

We present a series of L-Z plots in Figures 5 and 6. In order to illustrate the effect of using different R_{23} relations to compute the abundances for the more luminous galaxies we plot side-by-side the EP and KBG L-Z relations for each filter considered. In all plots, the solid line represents a weighted bivariate linear-least-squares fit to the data (using the bisector method). The uncertainties in the abundances are those specified in the previous section. For the uncertainties in the absolute magnitudes we adopt a conservative value of 0.3 mag. This reflects mainly the errors in the distances. The parameters of all of the linear-least-squares fits presented in this section are summarized in Table 6. The uncertainties listed in the table for the slopes and intercepts are the formal errors obtained from the fitting process. The errors are quite small due to the large sample of galaxies used. They may not reflect the true uncertainties in the coefficients, however. For example, the differences in the slopes of the direct and inverse fits are substantially

larger than the formal errors quoted in the table. We do not display the L-Z plots for the SDSS R_{23} calibration here, but include the results of the least-squares fits in Table 6. The appearance of the SDSS L-Z plots are very similar to the EP versions shown.

In most previous work, the B-band has been the filter of choice for the construction of L-Z relations. This is presumably due to the wealth of B-band photometry available for galaxies, but, as we shall see, it is perhaps a poor choice due to the severe effects of internal absorption plus the impact that extreme starbursts can have in the blue. The B-band L-Z relations shown in Figure 5a,b include all 766 KISS ELGs for which coarse abundances have been derived. There is a clear trend of increasing metallicity with increasing luminosity, as expected. The relations are well defined between $M_B = -16$ and -21 , where the bulk of the KISS sample is located. A modest number of dwarf galaxies extend down to $M_B = -14$, but these all lie above the best-fit lines. As suggested in Paper I, this may be an indication that the L-Z relationship flattens out at lower luminosities (i.e., the L-Z relation may not be strictly linear). The slope of the fitted line is -0.280 for the EP relation, and -0.222 for the KBG relation, both substantially steeper than B-band L-Z relations obtained in the past using primarily dwarf galaxy samples (e.g., Skillman, Kennicutt & Hodge 1989; Richer & McCall 1995; Paper III). The L-Z relation of Skillman

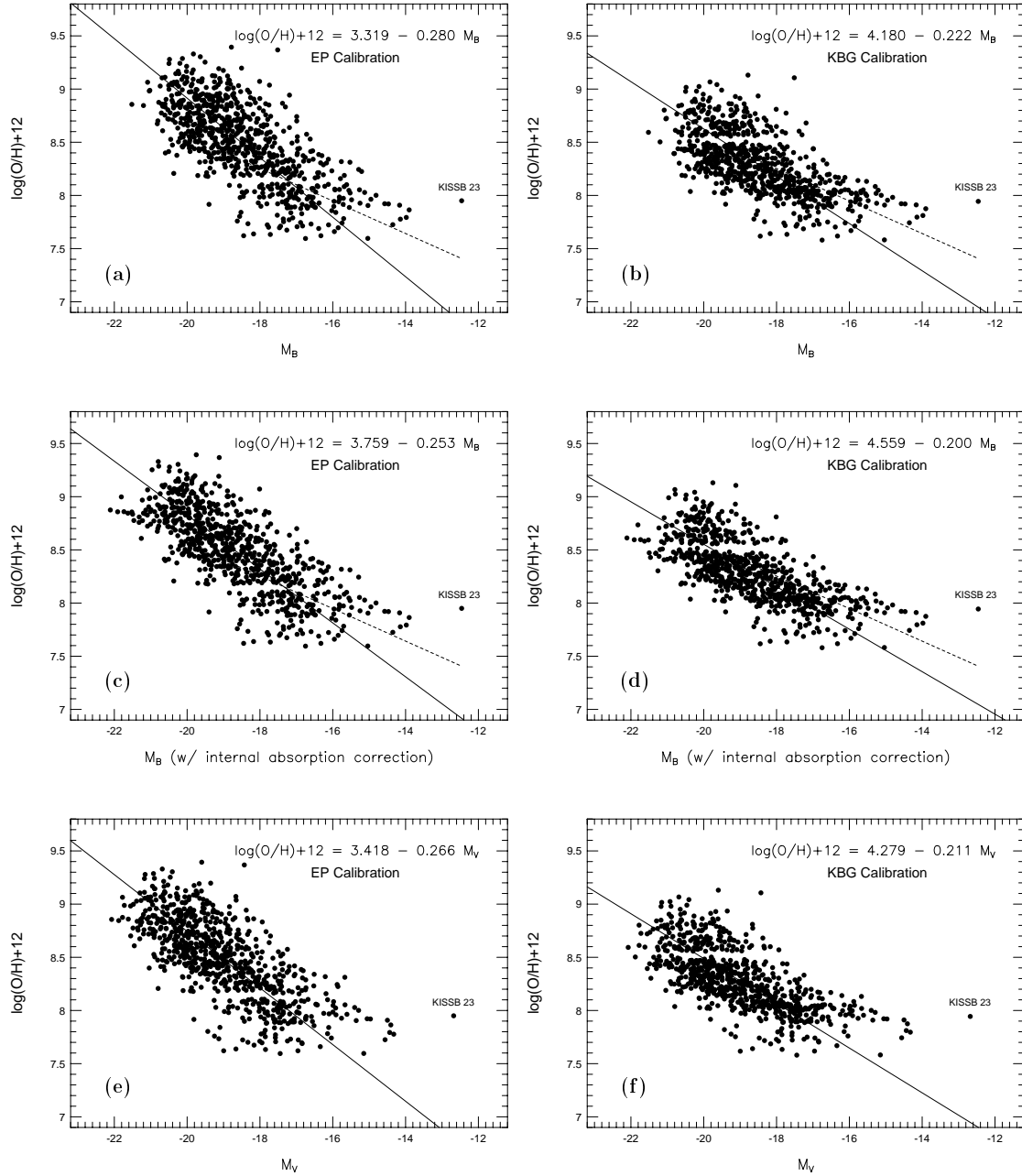


FIG. 5.— Optical luminosity-metallicity relationships for the star-forming KISS ELGs ($N=765$). Only galaxies with spectral qualities of 1 or 2 are included. The solid lines represent bi-variate linear-least-squares fits to the data, while the dashed lines are the L-Z relation found by Skillman, Kennicutt & Hodge (1989). Panels a) and b) show the B-band L-Z relations for the EP and KBG R_{23} calibrations respectively. Panels c) and d) are the same pair, with the only difference being that an internal absorption correction has been applied. Finally, panels e) and f) show the V-band L-Z relations for the EP and KBG relations.

et al. is shown in Figure 5a-d for comparison. The overall scatter in the O/H abundances about the fit line is 0.292 dex for EP and 0.245 dex for KBG. This is larger than the formal errors in our coarse abundances, and suggests that there is substantial “cosmic scatter” in the current relation. We will return to each of these last three points in the following section.

The location of the least luminous object in the figure, KISSB 23 (a very nearby dwarf ELG), is consistent with the idea that the L-Z relation may not be linear down to the lowest luminosities. It lies a full 1 dex above the extrapolation of the L-Z relation. We have labeled it in

Figure 5 because it appears to deviate so strongly from the relationship defined by the rest of the data set. Part of the reason this object is so discrepant may have to do with its evolutionary status. KISSB 23 has an extremely low-excitation spectrum compared to other dwarf ELGs. It is located well below the main locus of points in Figure 3 ($\log([\text{N II}]/\text{H}\alpha) \approx -1.45$ and $\log([\text{O III}]/\text{H}\beta) \approx 0.15$) and may be an aging starburst. Because of this, the coarse metal abundances based on the strong lines may be over-estimating the true metallicity. We can confirm this suggestion, since we have measured T_e abundances for KISSB 23 (Paper II, Paper III); the latter study finds

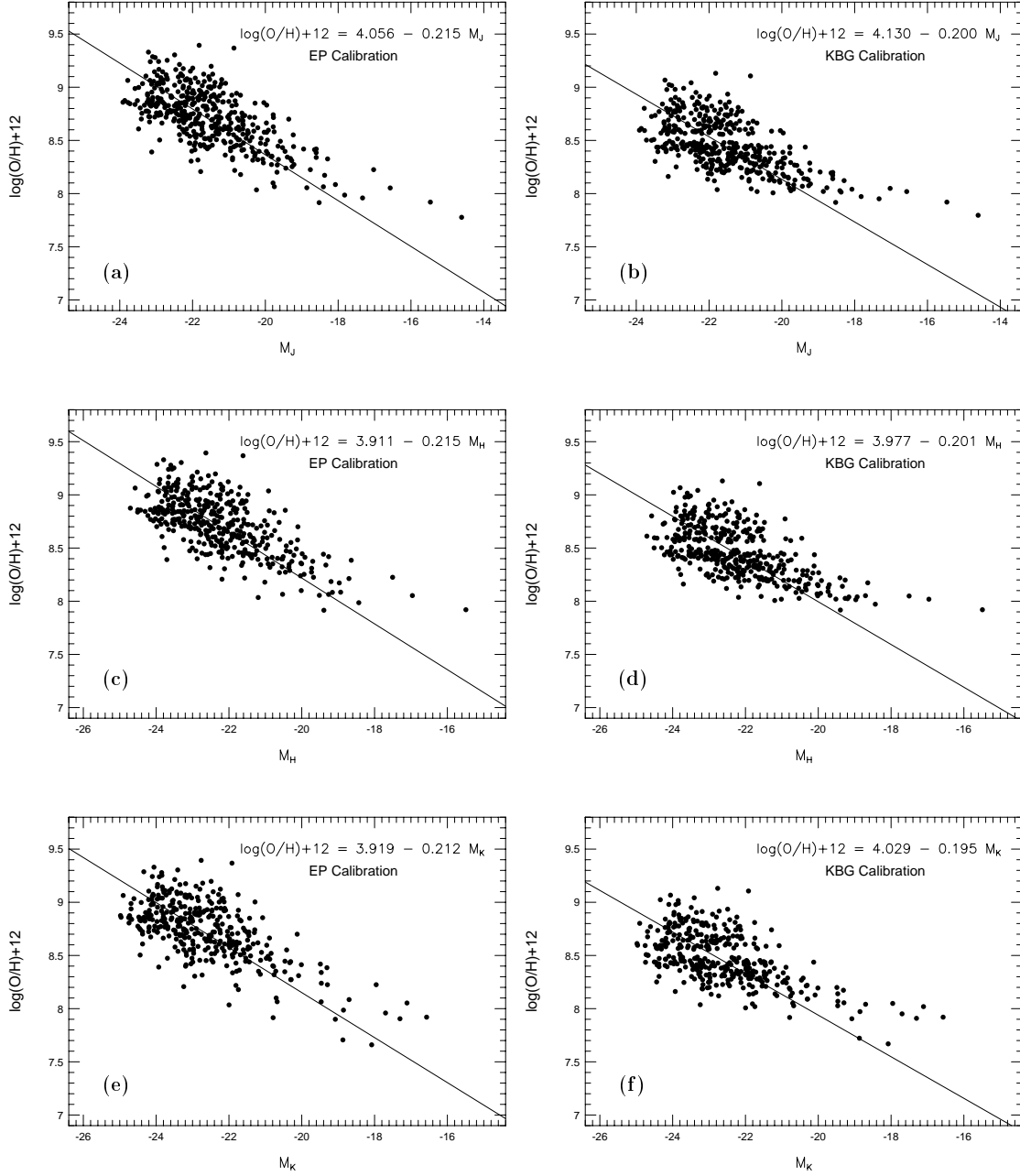


FIG. 6.— Near infrared luminosity-metallicity relationships for the star-forming KISS ELGs. Only galaxies with spectral qualities of 1 or 2 are included. The solid lines represent bi-variate linear-least-squares fits to the data. Panels a) and b) show the J-band L-Z relations for the EP and KBG R_{23} calibrations respectively ($N=420$). Panels c) and d) present the H-band relations for the EP and KBG relations ($N=399$). Finally, panels e) and f) show the K-band L-Z relations ($N=370$).

$12 + \log(O/H) = 7.65$, compared to 7.95 for our coarse abundance estimate (EP). Galaxies like KISSB 23 show the limitations of the strong-lined method for estimating abundances (R_{23} , p3, our method). Objects need to be near the peak of their star-formation episode (and on the main locus of points in line diagnostic diagrams like Figure 3) in order to generate accurate results from the strong-line abundance methods. KISSB 23 is one of only a small handful of objects in our sample which may fall in the category of “aging” starbursts. Therefore, we have not included it in any of our fits.

As noted in Paper I, one reason the slope of the KISS B-band L-Z relation is steeper than those of previous

studies is likely due to the fact that our sample contains a much higher proportion of luminous starburst galaxies, which in turn likely have a large amount of internal absorption that acts to decrease their observed luminosities. If this increased absorption occurs systematically at the high-luminosity end of the L-Z relation, then it will naturally lead to a steepening of the slope. Following the ad-hoc procedure described in Paper I, we can apply an internal absorption correction to the B-band absolute magnitudes and refit the data. Our results are displayed in Figure 5c,d. As expected, the slopes derived using the corrected luminosities are less steep (see Table 6). Furthermore, the overall scatter in the relationships

is reduced relative to the uncorrected fit.

The reason we would like to arrive at an absorption-free form of the L-Z relation is because such a relation should more nearly reflect the more fundamental relationship between metal abundance and mass. An obvious way to approach directly the ideal of an absorption-free L-Z relation is to measure the luminosity in longer wavelength photometric bands. The KISS data set includes V-band photometry, which provides a modest improvement over the B-band in this regard. However, real gains can be realized by moving into the NIR. Figures 5e,f and 6 show the KISS L-Z relations for the four photometric bands V, J, H, and K. As one would expect, the V-band relation (Figure 5e,f) is slightly less steep than for the uncorrected B-band (but more steep than the corrected B-band relation). Again, the relation is well defined over more than five magnitudes in absolute magnitude, and shows the same “turn up” at the low-luminosity end exhibited by the B-band relation.

The three sets of NIR L-Z plots (Figures 6) show a substantial change relative to the optical ones. Unfortunately, the number of KISS star-forming galaxies that also possess 2MASS photometry is only about half of the objects for which we have coarse abundance estimates. In the J-band L-Z plot (Figure 6a,b), for example, only 420 (55.0%) of the galaxies in the coarse abundance sample are included. Even lower numbers apply to the H-band (399 galaxies, or 52.2%) and K-band (370 galaxies, or 48.4%) data sets. Additionally, the NIR data are preferentially lacking at the lower luminosities, which motivated our efforts to obtain the additional NIR data presented in §2.3. Despite these constraints, the L-Z relations in the NIR bands are well defined.

Two key results are readily apparent in the NIR L-Z plots. First, all three exhibit substantially lower slopes than are present in the relations based on the optical data. For all three, the slope is approximately -0.21 (EP) or -0.20 (KBG). Second, the RMS scatter in the L-Z relations is significantly lower for the NIR data compared to the optical data, at least for the EP and SDSS fits. Both results can be interpreted as being due, at least in part, to the reduced effects of dust absorption in the NIR. The shallower slopes come about as the strong, luminosity-dependent absorption in the B and V bands is reduced to much lower levels in the NIR bands. Further, since the amount of absorption varies tremendously from galaxy to galaxy due to, for example, inclination effects, the scatter in the optical L-Z relation is presumably elevated. The lower scatter in the NIR relations is therefore a natural consequence of “removing” the variable amount of absorption. These results are consistent with the findings of Masters, Giovanelli & Haynes (2003), who show that, on average, the amount of internal dust absorption affecting disk galaxies is reduced to very low levels in the NIR compared to the optical. In particular, they suggest that the average level of absorption in the K band is only 0.1 mag. All appearances are that by producing a K-band L-Z relation we have achieved our goal of nearly eliminating the effects of absorption on the result.

4.2. The Impact of Using Different R_{23} Relations

We have computed our coarse abundances using three independent calibrations for the R_{23} relation in order to evaluate the impact that the different versions might

have on the derived L-Z relation. The main results of this test can be seen in Figures 5 & 6 and Table 6, which clearly indicate that the choice of which R_{23} relation to use for estimating the abundances of the high luminosity galaxies does have a significant impact on the slope of the resulting luminosity-metallicity relation.

Examination of Figure 5 shows the the L-Z relations derived using the KBG R_{23} calibration are systematically shallower than the EP versions. This is to be expected, since the abundances of the most luminous galaxies in the sample have abundances lower by 0.26 dex in the KBG relation. The slope differences average to ~ 0.055 dex for the three different relations plotted. Thus, if the KBG calibration is adopted over the EP calibration (or any of the other older determinations), the difference in the slope of the L-Z relation between our values based on EP and the “classical” Skillman, Kennicutt & Hodge value (-0.15) is effectively reduced by half. Interestingly, the slopes obtained using the SDSS calibration for the three optical L-Z relations are only slightly lower than the EP versions.

The differences between the L-Z relations derived with the three R_{23} calibrations are much smaller when the NIR relations are considered. The difference between the EP and KBG NIR slopes is only ~ 0.015 dex, with the EP relation still being the steeper of the two. The reason for the smaller slope difference in the NIR compared to the optical is not immediately obvious, but presumably is rooted in the vagaries of the sample differences between those KISS ELGs detected in the NIR and those that were not. Perhaps even more surprising are the very shallow slopes obtained using the SDSS NIR data. We interpret this as being due to the flatter nature of the SDSS R_{23} upper-branch relation (see Figure 2). We discuss this issue further in the following section. Why the *optical* SDSS L-Z fits agree so closely to the EP values, but then differ dramatically in the NIR, is again most likely an issue of the sample make up for the 2MASS-detected ELGs.

To summarize, we find significant differences in our derived L-Z relations depending on the choice of the R_{23} (upper branch) relation employed. At the moment there is no clear-cut “right” choice for which R_{23} relation to use. While the KBG version has the virtue of being based entirely on empirical data, the precise value of the derived relation is heavily constrained by the handful of most metal-rich H II regions observed. These observationally-derived abundances may well be uncertain, biasing the resulting R_{23} relation low. We point out, for example, that the KBG relation is 0.3 - 0.4 dex below two KISS ELGs with secure T_e -derived metallicities plotted in Figure 2. On the other hand, the model-dependent calibrations used in all of the older R_{23} relations (including EP) and by Tremonti *et al.* (2004) disagree with each other at a significant level, and hence it is difficult to place full faith in them as well. It is not the purpose of this paper to try to make a firm assessment of which R_{23} relation is the best. The answer to that question will likely require additional work - both observational and theoretical. Since our primary goal is to explore the nature of the L-Z relation, we are only concerned with the issue of how the different R_{23} relations impact the derived L-Z relation. Our findings should serve as a warning for future studies to carefully consider which R_{23} relation

to use and to take care when comparing with previous studies.

5. DISCUSSION

Despite the warnings issued in the previous section regarding the variations seen in our L-Z relations based on which R_{23} calibration we use, one can still draw firm conclusions regarding the nature of the L-Z relation. In the following discussion, we attempt to minimize the impact that the different R_{23} relations have by considering the broader nature of the L-Z relations we have derived. In essentially all cases, the qualitative results do not depend on the specific choice for the R_{23} calibration.

5.1. Comparison with Previous Studies and the Slope of the B-band L-Z relation

The results of Paper I and the current paper differ substantially from the classical L-Z studies of Skillman *et al.* (1989) and Richer & McCall (1995) in the sense that the slope we obtain for the B-band luminosity-metallicity relation is much steeper. For example, Skillman *et al.* obtain a slope of -0.153 and a scatter of 0.16 for their sample of 19 quiescent irregular and dwarf irregular galaxies. The recent study by H. Lee *et al.* (2003) obtains nearly identical results. In contrast, we find a slope of -0.280 (for the EP R_{23} calibration, -0.222 for the KBG calibration) and a scatter of 0.29 dex (EP, 0.25 dex for KBG). While part of the difference is due to the increased level of absorption in the higher luminosity galaxies in our sample, our attempt to correct for this only reduces the slope to -0.253 (EP, -0.200 for KBG). We plot the L-Z relation of Skillman *et al.* as a dashed line in Figures 5a-d.

We do not believe that the slope differences listed above reflect any systematic problems with the respective studies. In fact, when we use only the KISS galaxies with accurate T_e abundances from Table 2 to construct an L-Z relation, we obtain a fit with precisely the same slope as Skillman *et al.* (see Paper III). The galaxies in the latter sample cover the same absolute magnitude range as the Skillman *et al.* galaxies, and do not extend up into the higher luminosities present in our current sample. Therefore, we believe that the slope differences between these studies are real, and come about largely due to two factors: (1) The L-Z relation is not intrinsically linear over the full range of galaxian luminosities. Therefore, studies that cover different absolute magnitude ranges will arrive at different slopes. Recent studies involving large samples of galaxies have clearly revealed this non-linear nature at the high-luminosity end (e.g., Tremonti *et al.* 2004). (2) The amount of intrinsic absorption in a galaxy scales with its metallicity: high abundance galaxies will tend to have a higher molecular gas and dust content. Thus higher luminosity galaxies have luminosities that are systematically underestimated, which compresses the absolute magnitude range at the luminous end of the L-Z relation and artificially increases the slope. Since the Skillman *et al.* and Richer & McCall samples are made up of lower luminosity galaxies, they occupy a different portion of the L-Z diagram than does the bulk of the KISS sample. They also suffer less absorption than do the more luminous KISS ELGs. The two effects combine to produce a significantly shallower slope for these earlier studies, as well as for the subsample of KISS ELGs that cover a similar absolute magnitude range.

Another possible factor that could potentially produce a difference between our results and those of the previous studies mentioned above is the fact that we are using “coarse” abundances derived via strong emission lines, while the others are all using abundances derived using the T_e method. However, this difference does not appear to have a significant impact on the analysis. We have T_e abundances for 25 ELGs, taken mainly from Papers II and III. A comparison of the T_e and coarse abundances for these 25 sources shows that the two abundance estimates agree within the expected uncertainties. Specifically, the mean difference in $\log(O/H)$ between the T_e and coarse abundances is -0.009 dex, while the scatter about the mean is 0.163 dex (consistent with the uncertainty in the $[N II]/H\alpha$ coarse abundance method described in §3.3). Thus, over the abundance range covered by our sample of 25 T_e objects ($12 + \log(O/H) = 7.55 - 8.30$), our coarse abundance estimates are in good agreement, albeit with a large scatter.

Further evidence for a steeper L-Z slope can be seen in Zaritsky, Kennicutt & Huchra (1994). Using spectra of disk H II regions in a large sample of nearby spirals, they find that an L-Z relation exists for gas-rich galaxies that covers approximately nine magnitudes in M_B . While they state that their sample maps directly onto the L-Z relation defined by lower luminosity irregular galaxies, it is clear from their Figure 13 that the more luminous spirals are located systematically above the relation for the irregulars, indicating that a steeper slope is needed to fit the L-Z relation for the higher luminosity galaxies.

Garnett (2002) also considers the L-Z relation for a broad range of galaxian luminosities, but finds a slope comparable to that obtained by Skillman *et al.* (1989), Richer & McCall (1995), and H. Lee *et al.* (2003). This appears to be in direct conflict with our findings, in the sense that it negates the explanation given above for the slope differences between our work and the dwarf-only studies. Garnett’s sample includes many objects with M_B brighter than -20 . The key difference is that Garnett assigns a characteristic abundance for his larger spirals by evaluating the observed abundance gradient for each galaxy and adopting the O/H value measured at the half-light radius of the galaxy. In contrast, we derive abundances measured in the **central** star-forming complex of the KISS ELGs. Since the abundance gradients in spirals are typically significant (Zaritsky, Kennicutt & Huchra 1994; van Zee *et al.* 1998), the differences between our study and Garnett’s can be understood in terms of *where* the metal abundance is being measured in the galaxies. For example, in the sample of van Zee *et al.*, the abundance difference between the central value and the value measured at the half-light radius averages 0.34 dex (with the central value being higher). Adjusting the abundances of Garnett’s galaxies upward by 0.34 dex would clearly lead to a steeper L-Z slope. The question of where in the galaxy to measure the abundance is a valid one. Certainly one cannot fault Garnett for using the abundance measured part way out in the disk. For the KISS ELGs, on the other hand, the choice is dictated by where the star-formation event is occurring. For luminous ELGs, the emission-line region is essentially always in the central portion of the galaxy. We would argue that for comparison with most modern studies that

utilize fiber-fed spectrographs, and for comparison with studies of higher redshift galaxies, the use of centrally measured abundance values makes more sense.

Two recent studies have made use of much larger data sets to construct L-Z relations. Lamareille *et al.* (2004) utilize a sample of nearly 6400 galaxies from the 2dF Galaxy Redshift Survey to determine a B-band luminosity-metallicity relation. They select star-forming galaxies from the 2dF database that have strong nebular emission lines from which the O/H abundance can be derived using the R_{23} method (using the McGaugh 1991 calibration). They obtain an L-Z slope very similar to our value (-0.274) and find a scatter in their relation of 0.27 dex. Their sample contains a high percentage of luminous galaxies ($M_B < -18$): 92% of their objects are in the upper branch of the R_{23} relation.

Tremonti *et al.* (2004) use approximately 51,000 star-forming galaxies from the Sloan Digital Sky Survey (SDSS) to create a pseudo-B-band L-Z relation as well as a mass-metallicity relation. As with the KISS and 2dF galaxies, they derive their metal abundances using the strong nebular emission lines present in the spectra of their galaxies. A novel feature of the Tremonti *et al.* L-Z and mass-Z relations is that they flatten out at the highest luminosities/masses. This is readily understood in the context of the general picture that the L-Z relation reflects mainly a galaxy's ability to retain its own SNe ejecta, which depends primarily on the galaxian mass. Above some critical mass, essentially all of the metals produced in a galaxy will be retained. Hence, one would predict that for galaxian masses above this critical value, all galaxies will have the same relative metal abundance, and the L-Z and mass-Z relations should flatten out. This is exhibited dramatically with the SDSS data in Tremonti *et al.* ! Their mass-Z relation begins to flatten for masses above a few times $10^{10} M_{\odot}$. The flattening is less dramatic, but still evident, in their L-Z relation.

Given the clear evidence for the flattening at the high luminosity/mass end of the observed L-Z and mass-Z relations derived with the SDSS data, one must ask the question why a similar trend is not seen in the KISS data (or, for that matter, in the 2dF data). Comparison of our Figure 5a with Figure 4 of Tremonti *et al.* suggests the answer: the SDSS database systematically probes to higher luminosities than does KISS. While KISS has few star-forming galaxies with $M_B < -21$, the SDSS sample of Tremonti *et al.* shows large numbers of galaxies to $M_B = -22.5$. The differences between the two datasets are readily understood as sample selection biases. The spectroscopically observed portion of SDSS is a magnitude-limited sample, and hence includes many luminous galaxies at large redshifts. KISS, on the other hand, is a line-selected survey that has an inherent redshift limit of $z = 0.095$. Hence KISS does not probe to the large distances (and large volumes) that would allow it to detect large numbers of the relatively rare luminous galaxies. In addition, a second selection effect involves the ability to detect the line emission in KISS galaxies. The absolute strength of the emission lines emitted by a star-forming event will depend on several factors, but in general will scale with the size of the starburst. Depending on the size/luminosity of the host galaxy, that star-formation event will be detected as a KISS galaxy only if there

is sufficient contrast between the line and the underlying galaxian continuum. For extremely luminous host galaxies ($M_B < -21$), the underlying galaxy light tends to swamp the line emission from the starburst, making them difficult to detect. This selection effect means that KISS under-represents star-formation in the very most luminous host galaxies, unless the star-formation event is extremely strong. The two effects (lower volume surveyed for luminous galaxies and the contrast effect) together mean that KISS does not probe to the highest galaxian luminosities that SDSS reaches, which explains, at least in part, why we do not see the flattening in the KISS L-Z relation. The flattening is only present in the most luminous galaxies, and these are rare in the KISS sample.

The derived SDSS L-Z relation has a slope of -0.185 , which is considerably shallower than our result in the B-band but more consistent with the results of Skillman *et al.* (1989). Examination of their Figure 2 suggests a reason for this discrepancy. Tremonti *et al.* fit the entire dataset, including the portion with high luminosities where the correlation has begun to flatten out. It would appear that fitting only the galaxies with $M_B > -21$ would lead to a steeper slope. This has been confirmed by C. Tremonti (private communication), who fit the SDSS data after applying a selection function that more nearly mimics the type of selection relevant for the KISS ELGs. The resulting slope of -0.23 is steeper than their published value and lies closer to the value we arrive at in the current study.

The flattening of the Tremonti *et al.* L-Z and mass-Z relations, as well as their physical interpretation, needs also to be considered in the context of our earlier discussion regarding the specifics of the metallicity calibration used. The abundance determination method employed by Tremonti *et al.* utilizes the strong-line method but uses a more sophisticated scheme for deriving the metallicity. This method is model based, and yields an abundance calibration that tends to flatten dramatically at the upper end of the R_{23} relation (see their Figure 3). While this flattening is reasonable, if one were to utilize a linear upper-branch R_{23} relation (as we have for our EP and KBG fits), then the flattening observed at the highest luminosities in the L-Z relation essentially goes away (C. Tremonti, private communication). While we are not suggesting that the observed flattening in the Tremonti *et al.* L-Z and mass-Z relations is fictitious, it is worth remembering that this result does depend strongly on the specifics of the strong-line abundance calibration used.

5.2. The NIR L-Z relation

One of the key results of the current paper is the derivation of NIR luminosity-metallicity relations for our large sample of KISS star-forming galaxies. Other groups have considered the form of the L-Z relation in the NIR: Saviane *et al.* (2004) present an H-band relation for a small sample of Sculptor group galaxies, while Lilly, Carollo & Stockton (2003) display a J-band L-Z relation for their high redshift sample. Neither group generates a fit to their data, so we are unable to directly compare their relations with ours. To our knowledge, the NIR L-Z relations with fits shown in Figure 6 are the first ones ever published for a local sample of galaxies.

As discussed in §4, the main motivation for constructing L-Z relations in the NIR is to be able to avoid the effects of internal absorption on the high luminosity end of the relation. It is evident from the L-Z plots, as well as from the parameters of our linear-least-squares fits (Table 6), that the slope of the L-Z relation decreases monotonically as the wavelength of the photometric band used to construct it increases. Furthermore, the RMS scatter about the fit is reduced in the NIR relations. The similarity of the slopes for the three NIR bands suggests that it doesn't matter which band is used; the absorption effects are greatly diminished relative to the optical bands for all three.

Because the sample of galaxies used to construct our NIR L-Z relations changes significantly relative to the one used to derive the optical relations (e.g., §4.1 and Figure 4, we considered the possibility that the slope and RMS differences seen might be due to sample differences rather than being a real physical effect. To test this, we created a new B-band L-Z relation using only the 420 galaxies included in the J-band relation (Figure 6a,b). The fit to this data set yielded a slope of -0.307 ± 0.007 (EP calibration), slightly steeper than the value obtained with the full B-band sample (-0.280 ± 0.003). Furthermore, the RMS scatter for the new fit is 0.31 dex, compared to 0.29 dex for the fit to the full sample. *This result clearly shows that the differences in the L-Z relations between the optical and NIR are NOT due to sample issues.* In fact, one would have predicted just these results based on the interpretations given in the previous subsection. Since the NIR-detected sample is preferentially lacking in the lower luminosity galaxies, which are known to exhibit a shallower L-Z slope (see §5.1), the B-band L-Z slope for the J-band sample should be slightly steeper than the one for the full sample, as observed. Further, the J-band-detected objects, being more luminous, will suffer more from variable amounts of internal absorption, leading to a larger RMS than when compared with the full sample. Hence, we conclude that the shallower slopes and reduced RMS scatters exhibited by our NIR L-Z relations are real effects.

Another reason why the NIR L-Z relations are to be preferred over the optical ones is that variations in the NIR mass-to-light ratios (M/L) are substantially reduced relative to those in the optical (e.g., Bell & de Jong 2001). This is especially relevant if the underlying relation is one between mass and metallicity, as was assumed in §1. The primary effect of a smaller range of M/L values will be to further reduce the scatter in the L-Z relation by reducing the range in luminosities at a given mass. This comes about because the effect of variations in star-formation histories/stellar populations is less pronounced in the NIR than it is in the optical. This could be especially important for a sample of star-forming galaxies such as KISS (although see §5.3).

The slope of the L-Z relation might also be expected to be shallower in the NIR simply due to stellar population issues. As shown by Bell & de Jong (2001), the characteristic colors of galaxies vary smoothly with M/L ratio, in the sense that lower M/L values are bluer and higher M/L values are redder. Color and M/L ratio also correlate with luminosity, with bluer galaxies being less luminous and redder ones more luminous. As an example, a galaxy with $B-V = 0.3$ and $M_B = -16.0$ will

have a B-K color of ~ 2.3 and hence $M_K = -18.3$ (see Figure 9 of Bell & de Jong 2001). A galaxy with $B-V = 0.9$ and $M_B = -21.0$ will have $B-K \approx 3.9$ and $M_K = -24.9$. Hence, according to the models of Bell & de Jong, one would expect a shallower slope in the K-band L-Z relation since in this example $\Delta M_K = 6.6$ when in the optical for the same two galaxies $\Delta M_B = 5.0$. Presumably, both this effect and the lower amounts of absorption will both be acting simultaneously to reduce the observed slope in the NIR L-Z relation. It is not clear which effect will be the dominant one (or whether they will be of roughly equal magnitude). It is interesting to note that for the KBG R₂₃ calibration, the L-Z slope is identical for the absorption-corrected B-band relation and the NIR versions (Table 6). This implies that all of the slope change between the B-band and NIR relations is due to absorption effects. On the other hand, for both the EP and SDSS calibrations, the NIR L-Z slopes are significantly smaller than the absorption-corrected B-band values, suggesting that a sizable portion of the slope difference is due to the correlation between color and luminosity. Understanding the relative importance of the two effects will require additional work.

In the absence of absorption (e.g., Masters *et al.* 2003), the slope of the L-Z relation is -0.21 ± 0.01 (EP calibration). We suggest that this value is “fundamental,” in the sense that it reflects the change in abundance as a function of galaxian luminosity in the limit of zero absorption. To the extent that the L-Z relation is used to constrain models of galaxy evolution, the above slope would be the preferred value to use. While the ultimate goal would be to arrive at a relationship between mass and metallicity, in the absence of the former the NIR luminosity should be a robust substitute. This is because the NIR luminosities have a more direct correspondence to stellar mass than do optical luminosities. The latter suffer from the effects of higher absorption, plus optical mass-to-light ratios vary more than NIR ones due to stellar population differences. Thus the NIR luminosities are the preferred ones to use, and the NIR L-Z relations presented here are likely to be close to the ideal or fundamental relationships between luminosity and metallicity.

5.3. Scatter in the L-Z relation and 2nd parameter effects

Kobulnicky *et al.* (2003) searched for correlations between various parameters (color, emission-line equivalent width, effective radius) and residuals in their derived L-Z relationship in order to investigate whether there were any “second-parameter effects” that might be responsible for increased scatter in the L-Z relation. They found no significant correlations. In particular, they used the lack of correlation between $H\beta$ equivalent width and the L-Z residuals to argue that the presence of a strong starburst in some galaxies does not add dramatically to the observed scatter in the L-Z relation. While this result may appear to run counter to conventional wisdom, it is entirely consistent with what is observed in the KISS sample of local star-forming galaxies. For the luminous portion of the KISS sample ($M_B < -20$), even the most extreme starbursts rarely increase the total luminosity of the host galaxy by more than 0.2 magnitude in B (A. Jangren *et al.* 2005a, in preparation). In other words, we do not expect that the presence of starbursts in the KISS

galaxies to cause a significant increase in the scatter in the L-Z relation at the higher luminosities. Since the Kobulnicky *et al.* sample is confined to higher luminosities, they naturally do not see a significant trend. At lower luminosities the effect of a starburst on the luminosity of the host galaxy, and hence its position in the L-Z diagram, can be more significant (e.g., see Paper III). However, even in the cases of extremely powerful starbursts in low-luminosity hosts (a.k.a. blue compact dwarfs), the luminosity enhancement due to the starburst is usually under 1.0 magnitude in B (e.g., Salzer & Norton 1999).

We do see a significant reduction in the scatter in the L-Z relations derived using the KISS galaxies when the NIR luminosities are used. This suggests strongly that varying amounts of internal absorption in galaxies add significantly to the scatter in the B-band L-Z relation. As seen in Table 6, the RMS scatter in the KISS L-Z relation (EP calibration) drops from 0.29 dex for the uncorrected B-band relation, to 0.26 for the corrected B-band relation, to 0.22 for the J-band relation. The fact that the scatter increases slightly in going from J to H to K bands is likely due to the increasing photometric uncertainties present in the 2MASS photometry in the redder bands (see §2.2). As described above, the change in the derived slope for these fits is also consistent with a lowering of the internal absorption on the galaxian luminosities. We stress that this absorption effect does not alter the derived abundances, since the latter are corrected on a case-by-case basis for line-of-sight reddening based on their measured Balmer decrement. This is strictly a luminosity effect, which is why the scatter diminishes so dramatically between the B band and the NIR bands.

As discussed above, variations in the mass-to-light ratios of galaxies are expected to be lower in the NIR bands than in the bluer optical bands. It is likely that this effect also plays a role in reducing the scatter in the NIR L-Z relations. It is not clear how one could disentangle the two effects (absorption variations and M/L variations) with the present dataset.

A key question is whether or not the observed scatter in the NIR bands (0.22 – 0.23 dex) represents the fundamental “cosmic scatter” in the L-Z relation, or whether additional effects are acting to inflate the observed values. Since the formal errors in our abundance estimates are of order 0.15 dex (and may be somewhat higher if systematic effects are important), we are probably not in a position to explore this issue further with the current dataset. However, if we adopt our formal abundance error as being a lower limit to the actual uncertainties in our metallicity estimates, we can set an upper limit on the cosmic scatter in the L-Z relation of ~ 0.16 dex. The lack of any strong correlations between the residuals in the J-band L-Z relation and $H\alpha$ equivalent width, $c_{H\beta}$, and B–V color suggest that the observed scatter is not caused primarily by the current star-formation processes. Tremonti *et al.* (2004) report that their metallicity residuals correlate fairly strongly with the central surface mass density of their sample galaxies. This makes perfect sense, since if the L-Z relation is caused by mass-dependent variations in the ability of different galaxies to retain their SNe ejecta, then variations in the relation at a given mass/luminosity could naturally be caused by variations in the *mass distributions* of the galaxies.

In other words, for galaxies of the same mass, those with higher central mass densities should have modestly higher abundances. The proper resolution of this issue will require additional work employing samples with more precise abundance estimates (e.g., Tremonti *et al.* 2004).

5.4. High redshift L-Z relations

Tracking the build-up of metals in galaxies over cosmic time has recently become a realistic goal in the study of galaxy evolution. Several groups have recently explored the change in the metal content of galaxies with increasing redshift/look-back time (e.g., Lilly, Carollo & Stockton 2003; Kobulnicky *et al.* 2003; Maier, Meisenheimer & Hippelein 2004, Liang *et al.* 2004). With the establishment of a well-defined local L-Z relation, such as we have presented here, it becomes possible to explore the evolution of the relation as a tool for probing the chemical (and possibly star-formation) evolution history of galaxies. However, the results to date are, to say the least, confused. For example, the Maier, Meisenheimer & Hippelein and Liang *et al.* studies both report that the galaxies in their sample exhibit metallicity increases of about a factor of 2 between $z \approx 0.7$ and today, while Kobulnicky *et al.* find more modest increases and Lilly, Carollo & Stockton suggest that almost no metallicity enhancement has occurred over the same range of look-back times.

The task of making a self-consistent comparison between our new L-Z relations and the high redshift studies mentioned above is beyond the scope of the current paper. While one might be tempted to simply compare the various results on face value, a more careful approach is called for. The comparison between our L-Z relation and the one derived from SDSS data (Tremonti *et al.* 2004) serves as a clear example (see §5.1). While a direct comparison of the L-Z fits to the two datasets suggest discrepant results, a more careful analysis that treats the data in similar ways and accounts for sample selection differences arrives at very similar L-Z fits.

The lessons we have learned from the comparison of purely local L-Z relations suggest some of the elements that are necessary for a study that seeks to measure the global chemical evolution in galaxies by contrasting L-Z relations at different epochs. These include: (1) *Estimating abundances for all datasets in identical ways.* This would require starting with the observed line ratios and processing the high- and low- z samples following similar procedures. Relevant issues here include accounting for internal absorption (difficult for high- z objects since $H\alpha$ is often redshifted out of the spectral bandpass, but crucial since abundance estimates of high- z objects often rely on the $[O\ II]/H\beta$ ratio which is extremely sensitive to absorption), and the consistent use of the same R23 (or equivalent abundance estimator) calibration. (2) *Proper corrections to rest-frame luminosities.* While in principle this is very straight-forward (e.g., using standard k -corrections), one needs to be concerned about issues like the variable amount of absorption present in individual galaxies. In practice, the best approach would be to use multi-band imaging (which is often available for deep survey fields), fit the SED, and then derive the appropriate rest-frame magnitude from the SED fit. (3) *Use of similar fitting methods for the L-Z relations.* Different au-

thors tend to use different methods for fitting their data. To be assured that the fitting process does not introduce differences, it is always advisable to use the same fitting software/method for both high- and low- z L-Z relations. (4) *Recognizing and accounting for sample differences.* As with most studies of extragalactic objects, one must always be careful to avoid comparing “apples and oranges.” Since high- z samples tend to be dominated by higher luminosity galaxies, care must be taken to ensure that the local comparison sample has a similar make up.

The prospect of using L-Z relations measured at a range of redshifts as a tool for probing the chemical evolution of galaxies is an exciting one. While only in its infancy, this technique offers great promise for our understanding of galaxy evolution as well as the star-formation history of the universe. However, as outlined above, great care is required to avoid drawing incorrect conclusions.

6. SUMMARY & CONCLUSIONS

We use the large sample of nearby ($z < 0.095$) star-forming galaxies from the KISS objective-prism survey to explore the relationship between metallicity and luminosity. The homogeneous nature of the KISS follow-up spectra, combined with the depth and uniformity of the sample make this an excellent dataset to use for this purpose. We extend the analysis presented in Paper I by (i) using an expanded sample of KISS star-forming galaxies with the necessary follow-up spectra, (ii) re-determining the coarse abundance relations with a much larger sample of objects with quality abundance estimates, (iii) exploring the effect of using different R_{23} calibrations on the resulting L-Z relation, and (iv) evaluating the L-Z relation in five different photometric bands (BVJHK).

Follow-up spectra of a total of 766 KISS star-forming ELGs enable us to estimate abundances via a coarse (or strong-lined) abundance method. These objects also have accurate B and V photometry. By correlating the KISS catalog with the 2MASS database, we obtain NIR magnitudes for a subset of these KISS ELGs: 420 with J-band photometry, 399 with H-band data, and 370 with K-band magnitudes.

We demonstrate that testing the effect of using different strong-line method calibrations on the resulting L-Z relations is important and necessary, and expand our analysis from Paper I to include a range of proposed R_{23} -method calibrations. These result in significant variations in our derived L-Z relation fits. While the range in the derived L-Z slopes is significant, especially in the optical, we do not believe that it changes any of our general conclusions.

We present L-Z relations for all five photometric bands. In all cases the relations are derived using data that cover more than six magnitudes, or a factor of 250 in luminosity. We find that the slopes of the L-Z relations change systematically from the shortest to the longest wavelengths, in that the relation is steepest in the blue and most shallow in the near-IR. The RMS scatter in our relations decrease dramatically between the blue and NIR. We interpret these effects as being due, in large part, to the changing influence of internal absorption on the intrinsic brightnesses of the luminous portions of the galaxy populations as a function of the observed wavelength. In addition, changes in the contributions of the various stellar populations present in these galaxies (e.g.,

starburst population vs. older stars) to the various band-passes likely contributes to the observed slope changes as well.

The slope of our derived B-band L-Z relation differs dramatically from those obtained in some previous studies (e.g., Skillman *et al.* (1989); Richer & McCall 1995). The main difference is that we obtain a much steeper slope in the optical. However, those studies considered only low luminosity galaxies (typically $M_B > -18$), while the KISS sample ranges from $M_B = -14$ to -21.5 . Recent studies that cover a similar luminosity range also derive larger slopes (e.g., Lamareille *et al.* 2004). While part of the difference between our results and previous work may be due to absorption effects in the more luminous galaxies, it appears that the general L-Z relation is steeper than the value obtained using only low-luminosity galaxies. We suggest that the K-band slope of -0.21 represents a “fundamental” form of the L-Z relation. The fact that the slope derived using low-luminosity galaxies is less steep (-0.15) suggests that the L-Z relation is not linear over the full range of galaxian luminosities. The large scatter in our data, combined with the relative paucity of galaxies with luminosities below $M_B = -16$, makes it impossible for us to explore the non-linear nature of the L-Z relation with the current dataset. However, a clear hint of this nature can be seen in the L-Z and mass-Z relations derived recently by Tremonti *et al.* using the extensive SDSS database.

The determination of accurate L-Z relations provides fundamental input to our understanding of galaxy evolution. The fact that metal abundance correlates with galaxian luminosity (and mass) over essentially the entire range of the latter suggests that there are important constraints on the supernova feedback processes occurring within galaxies. Furthermore, the observed dispersion in the L-Z relation sets limits on the range of variation of these feedback mechanisms from galaxy to galaxy. Together, they provide important constraints to models of the chemical evolution of galaxies (e.g., Prantzos & Boissier 2000; Boissier *et al.* 2003; Chiappini, Romano & Matteucci 2003; Rieschick & Hensler 2003; Qian & Wasserburg 2004). In addition, recent studies have started to reveal the utility of using the L-Z relation as a tool for measuring the evolution of metal abundances in galaxies as a function of look-back time.

We gratefully acknowledge financial support for the KISS project from an NSF Presidential Faculty Award to JJS (NSF-AST-9553020), as well as continued support for our ongoing follow-up spectroscopy campaign (NSF-AST-0071114). JCL acknowledges financial support from NSF grants AST-9617826 and AST-0307386 as from a UA-NASA Space Grant Graduate Fellowship. We would also like to recognize and thank the members of the 2MASS project for producing such an excellent, useful, and highly accessible data set for the community. We are grateful for the assistance of Sun Mi Chung, Joseph Martin, and Anthony Moeller who helped with the analysis of the 2MASS data. We thank Don McCarthy for the use of his PISCES NIR camera, as well as George and Marcia Rieke for the use of their 256×256 NIR camera. Our NIR observations would not have been possible without these instruments and the respec-

tive PI's technical support during our runs. We thank the many KISS team members who have participated in the spectroscopic follow-up observations during the past several years, particularly Caryl Gronwall, Drew Phillips, Gary Wegner, Jessica Werk, Laura Chomiuk, Kerrie McKinstry, Robin Ciardullo, Jeffrey Van Duye and Vicki Sarajedini. We benefited greatly from helpful conversations with Christy Tremonti, Don Garnett,

and Rob Kennicutt. Many useful suggestions by the referee, Chip Kobulnicky, helped to improve the presentation of this paper. Finally, we wish to thank the support staffs of Kitt Peak National Observatory, Lick Observatory, the Hobbey-Eberly Telescope, MDM Observatory, and Apache Point Observatory for their excellent assistance in obtaining the spectroscopic observations that made this work possible.

REFERENCES

- Bell, E. F., & de Jong, R. S. 2001, *ApJ*, 550, 212
 Boissier, S., Monnier Ragaigine, D., Prantzos, N., van Driel, W., Balkowski, C., & O'Neil, K. 2003, *MNRAS*, 343, 653
 Chiappini, C., Romano, D., & Matteucci, F. 2003, *Ap&SS*, 284, 771
 Contini, T., Treyer, M. A., Sullivan, M., & Ellis, R. S. 2002, *MNRAS*, 330, 75
 de Robertis, M. M., Dufour, R. J., & Hunt, R. W. 1987, *JRASC*, 81, 195
 Edmunds, M. G., & Pagel, B. E. J. 1984, *MNRAS*, 211, 507 (EP)
 Garnett, D. R. 2002, *ApJ*, 581, 1019
 Garnett, D. R., & Shields, G. A. 1987, *ApJ*, 317, 82
 Garnett, D. R., Shields, G. A., Skillman, E. D., Sagan, S. P., & Dufour, R. J. 1997, *ApJ*, 489, 63
 Gronwall, C., Salzer, J. J., Sarajedini, V. L., Jangren, A., Chomiuk, L., Moody, J. W., Frattare, L. M., & Boroson, T. A. 2004a, *AJ*, 127, 1943 (KR2)
 Gronwall, C., Jangren, A., Salzer, J. J., Werk, J., & Ciardullo, R. 2004b, *AJ*, 128, 644
 Hidalgo-Gomez, A. M., & Olofsson, K. 1998, *A&A*, 334, 45
 Hodapp, K. W., *et al.* 1996, *NewA*, 1, 177
 Izotov, Y. I., Thuan, T. X., & Lipovetsky, V. A. 1997, *ApJS*, 108, 1
 Kennicutt, R. C., Jr., Bresolin, F., & Garnett, D. R. 2003, *ApJ*, 591, 801 (KBG)
 Kewley, L. J., & Dopita, M. A. 2002, *ApJS*, 142, 35
 Kobulnicky, H. A., & Zaritsky, D. 1999, *ApJ*, 511, 118
 Kobulnicky, H. A., *et al.* 2003, *ApJ*, 599, 1006
 Kozlowski, L. J., *et al.* 1994, *Proc. SPIE*, 2268, 353
 Lamareille, F., Mouhcine, M., Contini, T., Lewis, I., & Moddox, S. 2004, *MNRAS*, 350, 396
 Lee, H., McCall, M. L., Kingsburgh, R. L., Ross, R., Stevenson, C. C. 2003, *AJ*, 125, 145
 Lee, J. C., Salzer, J. J., & Melbourne, J. 2004, *ApJ*, 616, 752 (Paper III)
 Lequeux, J., Rayo, J. F., Serrano, A., Peimbert, M., & Torres-Peimbert, S. 1979, *A&A*, 80, 155
 Liang, Y. C., Hammer, F., Flores, H., Elbaz, D., & Cesarsky, C. J. 2004, *A&A*, 423, 867
 Lilly, S. J., Carollo, C. M., & Stockton, A. N. 2003, *ApJ*, 597, 730
 Mac Low, M., & Ferrara, A. 1999, *ApJ*, 513, 142
 Maier, C., Meisenheimer, K., & Hippelein, H. 2004, *A&A*, 418, 475
 Masters, K. L., Giovanelli, R., & Haynes, M. P. 2003, *AJ*, 126, 158
 McCall, M. L., Rybski, P. M., & Shields, G. A. 1985, *ApJS*, 57, 1
 McCarthy, D. W., Ge, J., Hinz, J. L., Finn, R. A. & de Jong, R. S. 2001, *PASP*, 113, 353
 McGaugh, S. S. 1991, *ApJ*, 380, 140
 Melbourne, J., & Salzer, J. J. 2002, *AJ*, 123, 2302 (Paper I)
 Melbourne, J., Phillips, A. C., Salzer, J. J., Gronwall, C., & Sarajedini, V. L. 2004, *AJ*, 127, 686 (Paper II)
 Oey, M. S. & Kennicutt, R. C. 1993, *ApJ*, 411, 137
 Osterbrock, D. E. 1989, *Astrophysics of Gaseous Nebulae and Active Galactic Nuclei* (University Science Books, Mill Valley, CA)
 Pérez-González, P. G., Gil de Paz, A., Zamorano, J., Gallego, J., Alonso-Herrero, A. & Aragón-Salamanca, A. 2003a, *MNRAS*, 338, 508
 Pérez-González, P. G., Gil de Paz, A., Zamorano, J., Gallego, J., Alonso-Herrero, A. & Aragón-Salamanca, A. 2003b, *MNRAS*, 338, 525
 Persson, S. E., Murphy, D. C., Krzeminski, W., Roth, M., & Rieke, M. J. 1998, *AJ*, 116, 2475
 Pettini, M., & Pagel, B. E. J. 2004, *MNRAS*, 348, 59
 Pilyugin, L. S. 2000, *A&A*, 362, 325
 Pilyugin, L. S. 2001, *A&A*, 369, 594
 Prantzos, N., & Boissier, S. 2000, *MNRAS*, 315, 82
 Qian, Y.-Z., & Wasserburg, G. J., 2004, *ApJ*, 612, 615
 Richer, M. G. & McCall, M. L. 1995, *ApJ*, 445, 642
 Rieschick, A., & Hensler, G. 2003, *Ap&SS*, 284, 861
 Salzer, J. J., Gronwall, C., Lipovetsky, V. A., Kniazev, A., Moody, J. W., Boroson, T. A., Thuan, T. X., Izotov, Y. I., Herrero, J. L., & Frattare, L. M. 2000, *AJ*, 120, 80
 Salzer, J. J., Gronwall, C., Lipovetsky, V. A., Kniazev, A., Moody, J. W., Boroson, T. A., Thuan, T. X., Izotov, Y. I., Herrero, J. L., & Frattare, L. M. 2001, *AJ*, 121, 66 (KR1)
 Salzer, J. J., Gronwall, C., Sarajedini, V. L., Lipovetsky, V. A., Kniazev, A., Moody, J. W., Boroson, T. A., Thuan, T. X., Izotov, Y. I., Herrero, J. L., & Frattare, L. M. 2002, *AJ*, 123, 1292 (KB1)
 Salzer, J. J., & Norton, S. A. 1999, in *The Low Surface Brightness Universe*, ASP Conference Series 170. Ed: J.I. Davies, C. Impey, and S. Phillipps p. 253
 Saviane, I., *et al.* 2004, in I.A.U. Symposium Series 217, *Recycling Intergalactic and Interstellar Matter*, ed. P. Duc, J. Braine, & E. Brinks.
 Shaw, R. A. & Dufour, R. J. 1995, *PASP*, 107, 896
 Skillman, E. D., Kennicutt, R. C., & Hodge, P. W. 1989, *ApJ*, 347, 875
 Skillman, E. D., Televich, R. J., Kennicutt, R. C., Garnett, D. R., & Terlevich, E. 1994, *ApJ*, 431, 172
 Stasinska, G. 1990, *A&AS*, 83, 501
 Tremonti, C. A., *et al.* 2004, *ApJ*, 613, 898
 van Zee, L., Salzer, J. J., Haynes, M. P., O'Donoghue, A. A., & Balonek, T. J. 1998, *AJ*, 116, 2805
 Wegner, G., Salzer, J. J., Jangren, A., Gronwall, C., & Melbourne, J. 2003, *AJ*, 125, 2373
 Zaritsky, D., Kennicutt, R. C., & Huchra, J. P. 1994, *ApJ*, 420, 87

TABLE 1
NEW H & K_S BAND PHOTOMETRY

KISSR (1)	KISSB (2)	H (3)	σ_H (4)	K _S (5)	σ_K (6)
286	133	14.60	0.06
310	136	16.92	0.07
311	137	16.49	0.08
314	138	12.98	0.19
396	145	15.16	0.06
505	161	14.30	0.30
666	186	17.59	0.11
678		16.24	0.20	15.34	0.06
742	192	16.53	0.38
998		16.07	0.39
1014		16.95	0.27
1091		16.45	0.45
1123	222	15.33	0.16

TABLE 2
METAL ABUNDANCES FROM THE T_e METHOD.

KISSR (1)	KISSB (2)	$\log([\text{N II}]/\text{H}\alpha)$ ^a (3)	$\log([\text{O II}]/\text{H}\beta)$ ^a (4)	$\log([\text{O III}]/\text{H}\beta)$ ^{a,b} (5)	12 + $\log(\text{O}/\text{H})$ (6)
...	23	-1.450	0.393	0.147	7.651
...	61	-2.160	0.142	0.652	7.763
...	71	-1.989	-0.087	0.722	7.660
...	86	-1.409	0.332	0.657	8.060
49	94	-1.099	0.537	0.515	8.000
73	98	-1.519	0.417	0.559	7.925
85	...	-2.444	0.069	0.483	7.606
87	104	-1.101	0.278	0.650	8.318
116	107	-1.196	0.304	0.641	8.071
286	133	-1.269	0.312	0.630	8.174
310	136	-1.940	-0.020	0.809	7.880
311	137	-1.539	0.378	0.693	7.981
396	145	-1.531	0.396	0.620	7.918
...	171	-1.416	0.263	0.686	8.114
...	175	-1.514	0.253	0.755	8.022
666	186	-2.166	-0.863	0.840	7.770
675	187	-1.706	0.103	0.752	7.866
814	199	-1.314	0.259	0.710	7.970
818	200	-1.280	0.459	0.779	8.307
1013	211	-1.259	0.320	0.592	7.658
1194	...	-1.506	0.311	0.709	7.918
1490	...	-1.606	0.179	0.590	7.563
1752	...	-1.897	0.038	0.553	7.569
1778	...	-1.295	0.447	0.461	7.928
1845	...	-1.429	0.385	0.723	8.047

^aAll line ratios are corrected for internal absorption using the measured value of $c_{H\beta}$. No corrections for underlying Balmer absorption have been applied.

^b $[\text{O III}]\lambda\lambda 5007/\text{H}\beta$

TABLE 3
METAL ABUNDANCES FROM THE p_3 METHOD.

KISSR (1)	KISSB (2)	$\log([\text{N II}]/\text{H}\alpha)$ ^a (3)	$\log([\text{O II}]/\text{H}\beta)$ ^a (4)	$\log([\text{O III}]/\text{H}\beta)$ ^{a,b} (5)	$12 + \log(\text{O}/\text{H})$ (6)
...	47	-1.782	0.148	0.682	7.794
96	105	-1.359	0.280	0.726	7.914
97	...	-1.337	0.493	0.628	8.049
105	...	-1.502	0.166	0.467	7.649
120	...	-1.367	0.167	0.675	7.800
223	127	-1.324	0.513	0.583	8.060
272	...	-1.528	0.359	0.476	7.849
343	140	-1.396	0.331	0.605	7.874
404	...	-1.489	0.459	0.456	7.972
405	147	-1.503	0.154	0.455	7.632
528	164	-1.437	0.507	0.582	8.053
715	190	-1.728	0.061	0.794	7.862
785	194	-1.565	0.287	0.760	7.945
803	...	-1.505	0.600	0.507	8.177
1021	...	-1.325	0.775	0.468	8.491
1177	...	-1.498	0.423	0.547	7.944
1794	...	-1.492	0.322	0.612	7.869

^aAll line ratios are corrected for internal absorption using the measured value of $c_{H\beta}$. No corrections for underlying Balmer absorption have been applied.

^b $[\text{O III}]\lambda 5007/\text{H}\beta$

TABLE 4
METAL ABUNDANCES FROM THE R_{23} METHOD.

KISSR	KISSB	$\log([\text{N II}]/\text{H}\alpha)^a$	$\log([\text{O II}]/\text{H}\beta)^a$	$\log([\text{O III}]/\text{H}\beta)^{a,b}$	EP	12 + $\log(\text{O}/\text{H})$ KBG	SDSS
(1)	(2)	(3)	(4)	(5)	(6)	(7)	(8)
1	...	-0.683	0.651	0.124	8.472	8.209	8.607
3	...	-0.571	0.729	-0.169	8.471	8.209	8.606
68	97	-0.787	0.426	0.413	8.484	8.222	8.619
91	...	-0.750	0.549	0.166	8.549	8.287	8.679
109	...	-0.527	0.506	0.201	8.568	8.305	8.695
110	...	-0.648	0.434	-0.109	8.777	8.514	8.857
117	...	-0.963	0.484	0.374	8.476	8.214	8.611
124	...	-0.859	0.506	0.372	8.463	8.201	8.598
133	...	-0.576	0.890	0.210	8.195	7.933	8.293
145	...	-0.368	0.420	-0.235	8.836	8.573	8.895
185	...	-0.533	0.355	-0.218	8.897	8.635	8.932
257	...	-0.811	0.562	0.308	8.461	8.199	8.597
265	...	-0.626	0.489	0.264	8.545	8.283	8.675
292	135	-0.736	0.522	0.480	8.374	8.112	8.507
317	...	-0.965	0.404	0.512	8.415	8.153	8.550
322	...	-0.413	-0.043	-0.564	9.427	9.164	9.149
326	...	-0.613	0.631	-0.005	8.538	8.276	8.669
327	...	-0.717	0.580	0.347	8.424	8.162	8.559
333	...	-0.325	0.430	-0.313	8.847	8.585	8.903
335	...	-0.384	0.386	0.233	8.641	8.379	8.757
368	...	-0.483	0.711	-0.296	8.515	8.253	8.648
398	...	-0.427	0.501	-0.145	8.721	8.458	8.817
400	...	-0.430	0.371	-0.364	8.926	8.663	8.949
515	...	-0.528	0.524	-0.058	8.667	8.405	8.777
520	...	-0.387	0.440	-0.157	8.788	8.526	8.865
577	...	-0.422	0.572	-0.235	8.668	8.405	8.778
582	...	-0.968	0.759	0.347	8.273	8.011	8.392
595	...	-0.399	0.005	-0.928	9.477	9.214	9.163
610	...	-0.662	0.461	0.077	8.671	8.408	8.780
643	182	-0.856	0.505	0.317	8.500	8.238	8.634
725	...	-0.634	0.348	0.191	8.696	8.433	8.799
830	...	-0.474	0.690	0.261	8.376	8.114	8.509
833	...	-0.542	0.566	-0.124	8.645	8.382	8.760
894	...	-0.493	0.614	-0.169	8.603	8.341	8.726
910	...	-0.566	0.416	-0.062	8.776	8.513	8.856
1016	...	-0.500	0.502	-0.131	8.715	8.453	8.813
1028	...	-0.362	-0.092	-0.597	9.488	9.225	9.165
1032	...	-0.723	0.520	0.170	8.572	8.310	8.699
1055	...	-0.466	0.550	-0.270	8.701	8.439	8.803
1062	...	-0.640	0.565	0.220	8.508	8.246	8.641
1402	...	-0.337	0.571	-0.634	8.734	8.472	8.827
1416	...	-0.719	0.615	0.200	8.473	8.211	8.608
1424	...	-0.292	0.490	-0.372	8.793	8.531	8.868
1537	...	-0.701	0.522	0.385	8.443	8.181	8.578
1885	...	-0.727	0.364	0.112	8.733	8.471	8.827
1940	...	-0.767	0.626	0.196	8.465	8.203	8.600
2021	...	-0.592	0.564	-0.041	8.621	8.358	8.740

^aAll line ratios are corrected for internal absorption using the measured value of $c_{H\beta}$. No corrections for underlying Balmer absorption have been applied.

^b $[\text{O III}]\lambda 5007/\text{H}\beta$

TABLE 5
COARSE METALLICITY RELATIONS

R_{23} Relation	A	B	C	RMS Scatter
(1)	(2)	(3)	(4)	(5)
[N II]/H α Relations				
EP	9.170 ± 0.070	1.094 ± 0.098	0.175 ± 0.033	0.136
KBG	8.578 ± 0.070	0.423 ± 0.098	-0.009 ± 0.033	0.156
SDSS	9.433 ± 0.070	1.391 ± 0.098	0.256 ± 0.033	0.130
[O III]/H β Relations				
EP	8.649 ± 0.022	-0.679 ± 0.068		0.144
KBG	8.386 ± 0.022	-0.679 ± 0.068		0.144
SDSS	8.732 ± 0.022	-0.450 ± 0.068		0.112

TABLE 6
RESULTS OF LINEAR FITS TO THE L-Z RELATIONS

Filter	Number	Slope	Slope Uncertainty	Intercept	Intercept Uncertainty	RMS Scatter
(1)	(2)	(3)	(4)	(5)	(6)	(7)
EP R_{23} Relation						
B	765	-0.280	0.003	3.32	0.06	0.292
B _o	765	-0.253	0.002	3.76	0.05	0.261
V	765	-0.266	0.002	3.42	0.05	0.274
J	420	-0.215	0.003	4.06	0.09	0.223
H	399	-0.215	0.003	3.91	0.09	0.225
K	370	-0.212	0.003	3.92	0.09	0.235
KBG R_{23} Relation						
B	765	-0.222	0.003	4.18	0.06	0.245
B _o	765	-0.200	0.002	4.56	0.05	0.219
V	765	-0.211	0.002	4.28	0.06	0.229
J	420	-0.200	0.004	4.13	0.09	0.222
H	399	-0.201	0.004	3.98	0.10	0.225
K	370	-0.195	0.004	4.03	0.10	0.233
SDSS R_{23} Relation						
B	765	-0.271	0.003	3.57	0.06	0.277
B _o	765	-0.247	0.002	3.96	0.05	0.251
V	765	-0.259	0.002	3.64	0.05	0.262
J	420	-0.173	0.003	5.03	0.08	0.165
H	399	-0.172	0.003	4.95	0.08	0.166
K	370	-0.173	0.003	4.85	0.09	0.179